Degenerate Four Wave Mixing in Biased Semiconductor Superlattices

by

Michael Sawler

Submitted to the Department of Physics
on 30 September 2001, in partial fulfillment of the
requirements for the degree of
Master of Science

Abstract

We present the first calculation of Degenerate Four-Wave Mixing(DFWM) in a Biased Semiconductor Superlattice. This calculation is done to third order in the electric field, using an exciton basis. We first develop the Hamiltonian for a biased semiconductor superlattice using the methodology of Dignam and Sipe, then, using the quasibosonic treatment of Hawton and Nelson, derive the correlation functions necessary to calculate the DWFM signal. We examine the absorption spectra, spectral power density, as well as the Time-Resolved and Time-Integrated DFWM signal intensity produced by our system, and find they are consistent with previous experimental and theoretical results. We also introduce a simplified version of the system of correlation functions using factoring. The terms to third order in the electric field are factored into a product of a first and second order term. A comparision of this with the full system is found to give good results.

Thesis Supervisor: Margaret Hawton
Title: Professor, Lakehead Univeristy

Thesis Supervisor: Marc Dignam
Title: Professor, Queen's University

Chapter 1

Introduction

Optical spectroscopy is a powerful tool for investigating the electronic properties of a variety of systems, and has provided extensive information and insights into the properties of atoms, molecules, and solids. In the field of semiconductor research, the techniques of absorption, reflection, luminescence and light-scattering spectroscopies have provided a great deal of information about such aspects of semiconductors as electronic band structure, phonons, single-particle excitation spectra of electrons and holes, coupled phonon-plasma modes, and the properties of defects and surfaces. These are essential contributions to our understanding of the physics behind semiconductors, but there is a great deal more which optical spectroscopy can do.

Optical spectroscopy also has several unique strengths which make it capable of providing information about the nonlinear, nonequilibrium, and the transport properties of semiconductors. These strengths, which when combined with pico- and femtosecond laser pulses, can provide new insights into completely different aspects of semiconductors, can be divided into four groups: (1) photoexcitation generates excitations, such as electrons, holes, phonons, and excitons, with non-equilibrium distribution functions, (2) optical spectroscopy also provides the best means of analyzing the distribution functions associated with these excitations, in order to determine the dynamics of the relaxation of these excited systems, (3) by combining optical spectroscopy with spatial imaging, we can investigate the transport of excitations, and the dynamics of the transport itself, in semiconductors and the nanostructures which can be made from them, i.e. quantum wells, superlattices, etc., (4) optical techniques provide the ability to

look into the nonlinear properties, including the coherent effects, in semiconductor structures, and thus provide insight into more aspects of them, such as many-body effects, coherence and dephasing phenomena. It is this area in which we are interested here.

The coherent regime is the temporal regime during and immediately following photoexcitation by an ultrashort laser pulse. In this regime, the excitations produced by the pulse still retain some definite phase relationship with the EM radiation that created them. The photoexcitation creates a macroscopic polarization in the system. This acts as a source term in Maxwell's equations, and determines the linear and nonlinear responses of the system to the excitation. Therefore, by investigating these responses, one can get information about the induced polarization, and hence about the coherent regime.

The coherent effects produced by photoexcitation in semiconductor superlattices and quantum wells have received considerable attention in recent years. Examples include the beating of light and heavy holes in quantum wells[1], wave-packet oscillations in coupled-double-quantum-wells[2], and Bloch oscillations[3]. These all involve creating excitons using ultrashort laser pulses with energies near the band gap. The resulting excitonic states have been examined experimentally via the degenerate four wave mixing (DFWM)[3], pump-probe spectroscopy, and the detection of terahertz radiation[4].

There has also been considerable effort devoted to treating these systems via theoretical methods. The most common approach to this has been to use the Semiconductor Bloch Equations (SBEs).[6] Other approaches range from utilizing phenomenological two- and three-level systems[2], to a more complete method, that of dynamically controlled truncation [7][8], and the quasibosonic methodology used by Hawton and Nelson[9]. The difficulty lies in developing a description which satisfactorily treats the electron-electron interactions present in these complex systems, while at the same time remaining simple enough to be computationally tractable.

In this thesis we present the first calculation of Degenerate Four-Wave Mixing in a biased Semiconductor Superlattice. This calculation is done using an exciton basis, working to third order in the optical field. The importance of phase-space filling to the overall DFWM signal is investigated. We develop both the full third-order calculation, as well as a simplified version involving the factorization of the third order terms into a product of first and second order terms. The results of calculations using the unfactored system of equations are then examined

and compared to previous results. We then compare the factored and unfactored versions over a variety of pulse time delays.

The remainder of this thesis is divided up into several chapters. Chapter 2 is devoted to describing the SBEs, the Wannier-Stark Ladder, and Bloch Oscillation theory used in our calculation. We also examine the theoretical and experimental work done in this area previously. Chapter 3 develops the equations of motion which allow us to calculate the DFWM signal for a biased semiconductor superlattice to third order in the electric field, and also the factorized version of these equations. Chapter 4 discusses the results of the calculation. Chapter 5 summarizes these results.

Chapter 2

Background Theory

In this chapter, we discuss the theory behind the Wannier-Stark Ladder (WSL), Bloch Oscillations, and Four-Wave Mixing experiments. We also discuss some of the theoretical and experimental work which has been done previously in this area. We begin by discussing the Semiconductor Bloch Equations.

2.1 Semiconductor Bloch Equations

The electron and hole states in a semiconductor span a wide range of energies and wavevectors. If only the lowest conduction band and highest valence band are considered, then each state will have a well-defined energy and momentum associated with it. In the absence of Coulomb interaction, one can then consider these continuum electron-hole pair states as being inhomogeneously broadened in momentum space. When the Coulomb interaction is included, this simple picture changes, to a series of bound states of the electron-hole pair, or exciton, and also affects the optical matrix elements corresponding to interband transitions involving the continuum states. These changes have profound impact on not only the linear properties of the semiconductor, but also the non-linear ones as well. The simplest approximation allows one to ignore all the continuum electron-hole pair states, considering only the ground state and one excited state, which corresponds to the bound 1s exciton state in which the oscillator strength is concentrated. If one ignores interaction between excitons, then a collection of excitons may be thought of as an ensemble of independent two-level systems. These systems

may be homogeneously or inhomogeneously broadened depending on the nature of the sample being investigated. In fact, many FWM experiments on semiconductors have been done using this simple model, and a great deal of useful information has been obtained. However, such an analysis cannot adequately describe everything which occurs in real semiconductors. In particular, one cannot ignore the interaction between the excitons themselves. These many-body interactions have been found to have a profound influence on the coherent nonlinear response of semiconductors.[5] In order to understand the nonlinear response, one must go beyond the assumption of independent two-level systems. This is where the Semiconductor Bloch Equations come into play.

In recent years, a theoretical framework to include the many-body Coulomb interactions has been developed[6]. We will not provide a full derivation here, but will rather give a brief description. Taking the Hamiltonian for a two-band system, we transform it into an electron-hole representation. The equations of motion are then derived for the following elements of the reduced density matrix associated with the Hamiltonian

$$\left\langle \alpha_{\mathbf{k}}^{\dagger}\alpha_{\mathbf{k}} \right\rangle = n_{e,\mathbf{k}}(t) \tag{2.1}$$

$$\left\langle \beta_{-\mathbf{k}}^{\dagger}\beta_{-\mathbf{k}} \right\rangle = n_{h,\mathbf{k}}(t) \tag{2.2}$$

$$\left\langle \beta_{-\mathbf{k}}\alpha_{\mathbf{k}} \right\rangle = \mathbf{P}_{\mathbf{k}}(t) \tag{2.3}$$

where

$$\alpha_{\mathbf{k}}^{\dagger} = a_{c,\mathbf{k}}^{\dagger} \tag{2.4}$$

$$\beta_{-\mathbf{k}}^{\dagger} = a_{v,\mathbf{k}}. \tag{2.5}$$

Here $\alpha_{\mathbf{k}}^{\dagger}$ corresponds to the creation of an electron in the conduction band with wave vector $\vec{\mathbf{k}}$, and $\beta_{-\mathbf{k}}^{\dagger}$ to the creation of a hole in the valence band with wave vector $-\vec{\mathbf{k}}$. By using a Hartree-Fock approximation[6], one splits the four operator terms in the equations of motion into products of densities and interband polarizations. After some substitutions, one arrives at

the following equations, which are the SBEs:

$$\frac{\partial \mathbf{P_k}}{\partial t} = -i\left(e_{e,k}+e_{h,k}\right)\mathbf{P_k} - i\left(n_{e,\mathbf{k}}+n_{h,\mathbf{k}}-1\right)\omega_{R,\mathbf{k}} + \left.\frac{\partial \mathbf{P_k}}{\partial t}\right|_{col} \tag{2.6}$$

$$\frac{\partial n_{e,\mathbf{k}}}{\partial t} = -2\,\mathrm{Im}\left(\omega_{R,\mathbf{k}}\mathbf{P}^*_{\mathbf{k}}\right) + \left.\frac{\partial n_{e,\mathbf{k}}}{\partial t}\right|_{col} \tag{2.7}$$

$$\frac{\partial n_{h,\mathbf{k}}}{\partial t} = -2\,\mathrm{Im}\left(\omega_{R,\mathbf{k}}\mathbf{P}^*_{\mathbf{k}}\right) + \left.\frac{\partial n_{h,\mathbf{k}}}{\partial t}\right|_{col} \tag{2.8}$$

where $\omega_{R,\mathbf{k}}$ is the generalized Rabi frequency, $e_{e,k}$ and $e_{h,k}$ are the renormalized single-particle energies, which include the carrier interactions in the Hartree-Fock approximation, and the factor $1 - n_{e,\mathbf{k}} - n_{h,\mathbf{k}}$ is the population inversion of the state $\mathbf{k}$. It's effects on the optical absorption spectra are often denoted as phase space filling.

These equations reduce to the optical Bloch equations for independent two-level systems when the Coulomb interaction between the excitons is removed. This corresponds to inhomogeneously broadened independent two-level systems in momentum space, which corresponds to the continuum states in the valence and conduction bands of a semiconductor in the absence of any Coulomb interaction.. Also, the homogeneous part of the equation for $\mathbf{P_k}$ becomes the generalized Wannier equation for electron-hole pairs.

The Semiconductor Bloch Equations described above form a cornerstone in the nonlinear optics of semiconductors. Despite their success in explaining numerous effects they have a significant disadvantage in that they are based on the ill-controlled Hartree-Fock approximation, as was mentioned above. The range of validity of the SBEs is not clearly defined because of this. In 1995, Axt, Bartels, and Stahl[8] showed this by comparing the SBEs with the complete second order solution of the underlying microscopic model for a biased semiconductor superlattice. In order to do this, they utilized a method known as dynamics controlled truncation (DCT) of the hierarchy of density matrices for optically excited semiconductors. The idea behind DCT relies on the observation that a complete calculation of the nonlinear optical response of a semiconductor to a given order in the driving field can be obtained by considering only a finite set of electronic correlation functions. They found that the differences between the SBE approach, and their more rigorous solution should be most pronounced (1) when the excitation is selective to states strongly affected by excitonic effects, and (2) when the system is far from

the so-called coherent limit. The Coulomb coupling of the electron and the hole within a pair in the SBE's decays faster than the intraband polarization, since the factorization implies that intraband processes decay twice as fast as the interband processes. This leads to the prediction that the THz emissions will have frequencies which are characteristic of free electrons and holes. However, experiments showed that in fact that the THz emission is dominated by excitonic processes[10].

In 1998, Hawton and Nelson [9] developed a hierarchy of equations describing the electrodynamics of the semiconductor band edge. They worked in a basis of Wannier excitons whose centers of mass were free to move about the crystal. These were described by exciton operators which is a sum of products of fermionic electron and hole creation operators. Excitons at low densities are bosons, and their creation and destruction operators can be shown to satisfy bosonic commutation properties to a first approximation. This is in direct contrast to the SBEs, which are primarily formulated in **k** space, where the free electrons and holes have fermionic properties. Working in the product space of fermions and quasibosons, they transformed the Hamiltonian from the fermion space of electrons and holes to the quasibosonic space of the excitons. Their system was consistent with that of DCT, and reduced to the SBE's when it was terminated at fourth order in the electric field. It also provided a simplified description of the physics of optical processes of semiconductors near the band edge. This process was applied to a superlattice subjected to combined static and terahertz along-axis electric fields by Lachaine et al.[11]

2.2 Wannier-Stark Ladder

The concept of the Wannier-Stark ladder (WSL) appeared in connection with the theoretical study of electronic bands in solids under the influence of an electric field. James[12] pointed out that an electric field should quantize the energies of the electrons in a band into discrete levels, each separated by $\Delta E = eFd$, where F is the applied static electric field, and d is the period of the crystal structure of the solid. The first mathematical treatment of this phenomena was conducted by Kane[13], and the term Stark ladder was introduced by Wannier[14]. However, experimental evidence of the existence of the Wannier-Stark ladder remained inconclusive for

some time, because the electric fields required to obtain a sufficient separation of the energy levels were so high as to lead to electrical breakdown.

Semiconductor superlattices proved to be the ideal systems to test these predictions. They have longer periods and narrower bands than bulk crystals, which made the localization length λ similar to the period d, allowing this phenomena to be observed. The effects of electric fields on superlattices was first investigated theoretically. McIlroy[15] used a superlattice consisting of four wells to numerically solve the Schrödinger equation. He obtained a finite Stark ladder whose levels split linearly with the field at high field strengths, and quadratically at lower fields. He was also able to obtain oscillations of the interband transitions. Bleuse et al.[16] used a finite many-well superlattice in a tight-binding approximation. This allowed them to predict a blue shift of the absorption edge and oscillations of the oscillations of the absorption which were periodic in F^{-1} for a constant photon energy.

The first experimental observations of the WSL in superlattices was reported by Mendez et al.[17] They were able to demonstrate the splitting of optical transitions, as well as the blue shift of the absorption edge. It was also found that the simplest technique to observe these phenomena was photoconductivity, which has been extensively used since. The absorption oscillations depending on F^{-1} were observed by Voisin et al. [18] via electroreflectance experiments. Since these, there has been a great deal of work done on the Stark ladder, from investigating different superlattice structures, such as GaAs/AlAs, and InGaAs, to measuring coherence lengths of electron wavefunctions and inducing doubly resonant Raman scattering by phonons.

Although these experiments were usually done at low temperature to reduce scattering effects, the WSL has been observed at room temperature[2]. Finally, the localization effects of the WSL has been used to create some superlattice-based electro-optic devices, such as modulators[2][**?**], and self-electro-optic effect devices[2], used in fiber-optics communications and optical computing.

The basic idea of the WSL can be qualitatively understood via the aid of Figure 2-1. When there is no electric field ($F = 0$), electron and hole levels in a superlattice form minibands with a dispersion relation due to the resonant coupling between the well levels. The period of the superlattice is $d = L_W + L_B$, where L_W and L_B represent the quantum well and barrier thicknesses, respectively. In an ideal superlattice, the levels of a given band correspond to

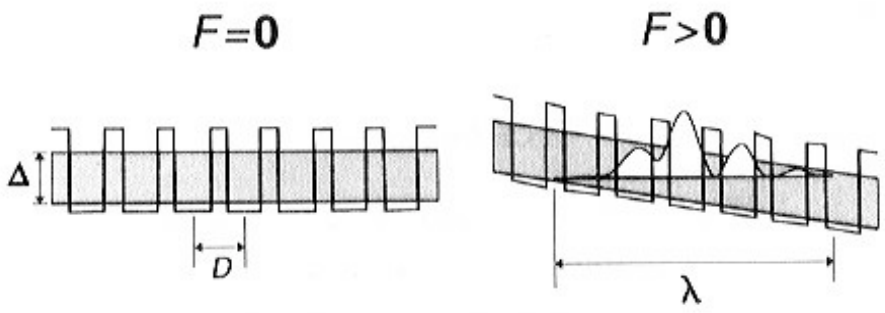

Figure 2-1: Schematic representation of the effects of an electric field applied perpendicular to the layers of a semiconductor superlattice on its electronic properties.(from [19])

states which extend over the entire structure. The superlattice states can thus be thought of as a superposition of the individual well states mixed by the resonance between the well levels. This is similar to how the electron states in a crystal can be considered as a superposition of atomic states.

When a constant electric field is introduced perpendicular to the layer planes, it introduces an electrostatic potential which detunes the interwell resonance, and 'tilts' the band. In the single-particle approximation the movement of a carrier in the z-direction of an intrinsic superlattice is described by Schrödinger's equation as seen here:

$$\left(-\frac{\hbar^2}{2m^*}\frac{\partial^2}{dz^2} + eFz + U(z)\right)\psi(z) = E\psi(z) \tag{2.9}$$

where $U(z)$ denotes the superlattice potential and m^* the bulk effective mass. Due to the electrostatic energy introduced by the electric field, a separation $\Delta E = eFd$ is created between single-well levels. This reduces the inter-well coupling due to the now imperfect resonance between levels. If ΔE becomes larger than the broadening of the single well levels, the miniband can be resolved into a Wannier-Stark Ladder. This ladder is formed by the levels of the N superlattice states, where N is the number of wells making up the superlattice. For an infinite superlattice, i.e. $N \to \infty$, edge effects are absent, and all of the levels become evenly spaced

out. At high enough fields, the levels of the WSL coincide with those of the single wells.

Due to the symmetry of the system, consecutive Stark ladder states have the same probability function, shifted only by one period in space., i.e.

$$|\psi_n(z)|^2 = |\psi_m(z-(n-m)d)|^2 \tag{2.10}$$

At a given electric field, the superlattice states will extend over a distance defined as the localization length, λ, where

$$\lambda = \frac{\Delta}{eF}, \tag{2.11}$$

and Δ is the miniband width. When F, the strength of the electric field, is on the order of Δ/ed, the localization length approaches one superlattice period. This is referred to as the complete localization regime, because at these levels of F, the probability function for the Stark ladder states are primarily confined to one well. This does not preclude them leaving that well, however.

In order to truly understand the Stark localization, one must solve the time-independent Schrödinger equation in the z-direction. This will yield the Stark ladder states. The approach we will use employs a tight-binding formalism. By using this method, we can obtain a very intuitive picture of the Wannier-Stark localization. We write the superlattice wavefunctions as linear combinations of all of the single-well wavefunctions $\phi(z-nd)$

$$\psi_m(z) = \sum c_{n-m}\phi(z-nd) \tag{2.12}$$

where if we only consider nearest-neighbor overlapping, and neglect the coupling with other bands, the c_{n-m} can be written as

$$c_{n-m} = J_{n-m}\left(\frac{\Delta}{2eFd}\right), \tag{2.13}$$

where J_n is the Bessel function of the first kind of order n. For cases when the miniband width,

$\Delta \ll 2eFd$, this expression can be approximated by the following:

$$J_{n-m}\left(\frac{\Delta}{2eFD}\right) = \frac{1}{|n-m|!}\left(\frac{\Delta}{4eFd}\right)^{|n-m|} \tag{2.14}$$

This function shows mathematically the WS localization. The wavefunction decreases at a faster than exponential rate as n and m move apart. Also, as the field increases,

$$c_{n-m} \to 1, \text{ if } n = m, \tag{2.15}$$

and

$$c_{n-m} \to 0, \text{ if } n \neq m. \tag{2.16}$$

This causes the superlattice state to localize in well m, becoming identical to the single-well state of that particular well. Heavy holes localize faster than light holes, due to their smaller bandwidth. The resulting eigenenergies are

$$E_m = E_1 + meFd \tag{2.17}$$

Note that this equation does not apply at low fields, due to the fact that it predicts the convergence of the ladder into a single energy value when the field becomes zero.

Each hole state n, overlaps with a number of electron states m, producing as many optical transitions labeled $(m-n)$. This is illustrated in the diagram below. If $n = m$ then the electron and hole states correspond to the same well and the transition is defined as intrawell, as opposed to the interwell transitions which occur between states corresponding to different wells $(n \neq m)$. If the electric field is constant throughout the superlattice, then transitions with the same $p = m - n$ are identical, and the energies depend only upon the separation between the electron and hole well. This leads to

$$E_p(F) = E_0(F) + peFD \tag{2.18}$$

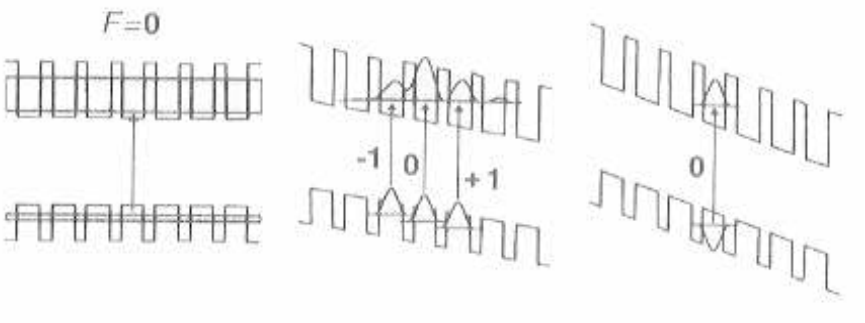

Figure 2-2: Sketch showing the origin of interwell transistions between different Stark Ladder states. The labels give the index p. (from [19])

where $E_0(F)$ is the intrawell transition energy

$$E_0(F) = E_g + E_{1e}(F) + E_{1h}(F) \tag{2.19}$$

where E_g is the band gap of the well bulk semiconductor. The field dependance of $E_0(F)$ comes from the Stark effect on a single quantum well. In superlattices, the wells are usually too narrow to achieve strong coupling, This results in small Stark shifts, and E_0 becomes nearly field independent. The interwell transition energies move linearly with the field as it is observed by experiment. This is illustrated in Figure 2-2. One should note that the energies plotted are actually excitonic peaks. Excitonic effects introduce some corrections to the single particle approximation, and will be discussed next.

2.2.1 Excitonic Effects

The Coulomb interaction between electrons and holes creates an exciton peak which is slightly below that of the single-particle interwell transition E_p. This peak corresponds to the $1s$ state of the exciton, and the separation from E_p is the exciton binding energy $E_b^p(F)$. The interwell exciton transition energies, $E_p^x(F)$ is given by the following

$$E_p^x(F) = E_0(F) - E_b^p(F) + peFD. \tag{2.20}$$

Note that this is simply the interwell transition energy from the previous section, minus the exciton binding energy.

The exciton effects have been calculated in detail as a function of field by several authors. Also, the influence of the superlattice period has been considered as well. Figure 2-3 below shows the binding energy calculated for a typical superlattice, showing the energies associated with several different interwell transitions, as well as the intrawell transition. As you can see, the binding energy for the intrawell exciton at high fields increases. At lower fields, it oscillates with the field strength due to the nodes in the wavefunction of the Stark ladder in a similar manner to the single-particle oscillator strength.

The interwell exciton binding energies, on the other hand, reach a maximum value,and then decreases asymtoticly to a constant value. This maximum occurs for the field where the probability of finding both the electron and hole in the same well is largest. The strength of this field decreases as $|p|$ increases. Close to this maximum, the binding energies for the $p \neq 0$ states differs based on the period of the superlattice. For long-period superlattices, the binding energies are larger for excitons with $p < 0$, whereas for short-period superlattices, the opposite occurs.[20]

2.3 Bloch Oscillations

In 1928, Bloch demonstrated theoretically that an electron wavepacket composed of a superposition of states from a single band and a given quasi-momentum $\mathbf{k}$ will undergo periodic oscillations in real and momentum-space under an applied electric field.[21] The period of these oscillations, τ_B, is inversely proportional to the applied field, F, and the periodicity of the crystal lattice, d, in the field direction. This concept has sparked a great deal of controversy over the decades, centering around the proper theoretical approach to describe the motion of an electron in an infinite solid under an applied electric field and the existence of a discrete WSL in a solid. From a theoretical point of view, it appears that the original picture of a discrete WSL is correct approximately. However, these states are metastable, due to the decoupling between states in different bands. However, on the experimental side, neither Bloch oscillations or the WSL have been demonstrated in bulk solids.

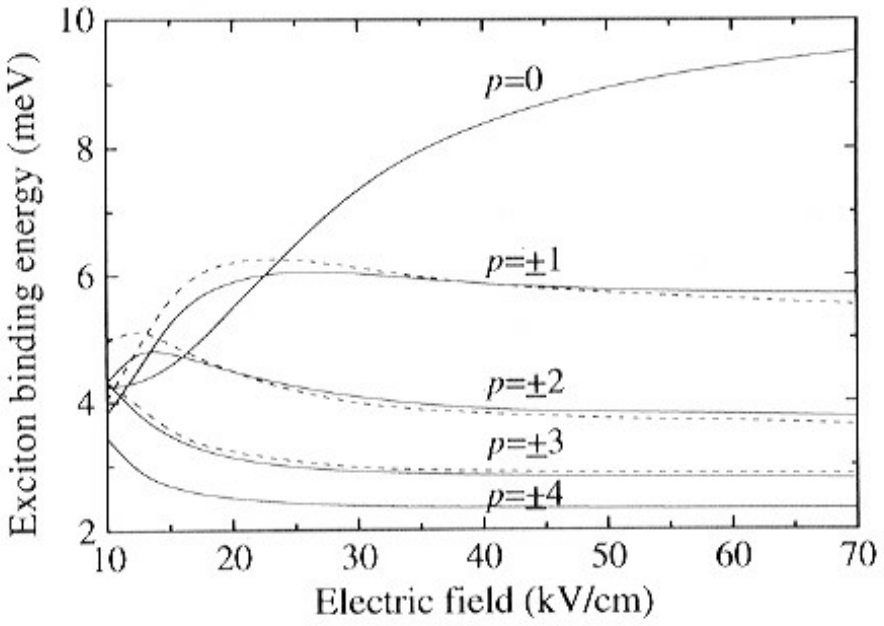

Figure 2-3: Binding energies for interwell excitons calculated as a function of the applied electric field for a superlattice. The dashed lines represtent the transitions where $p < 0$. (from [19])

One of the conditions for the observation of Bloch Oscillations (BO) is that the oscillation period, τ_B, must be smaller than the dephasing time τ_2.[22] One of the mechanisms governing τ_2 is interband tunneling, which becomes more important as the applied field increases. Since d can be much larger in superlattices than in bulk solids, the Bloch oscillation period can be much smaller than the corresponding period in a bulk solid for a given electric field. This makes superlattices ideal candidates for the observation of the WSL and Bloch oscillations.

Bloch oscillations can most easily be understood using semiclassical theory. In a semiclassical picture, the rate of change of the quasi-momentum in an applied field F is given by

$$\hbar\dot{k} = \mathbf{eF} \tag{2.21}$$

so that

$$k = k_0 + eFt/\hbar \tag{2.22}$$

The time it takes to go from $-\pi/d$ to π/d is τ_B, the Bloch oscillation period, which is also given by h/eFd. If the dispersion relation for the miniband is given by

$$E = E_0 - \frac{\Delta}{2}\cos(kd) \tag{2.23}$$

then the group velocity, given by $(\partial E/\partial k)/\hbar$, and the position z of the wavepacket can be found via

$$v(t) = \frac{\Delta d}{2\hbar}\sin\left(\frac{2\pi t}{\tau_B}\right) \tag{2.24}$$

and

$$z(t) = z_0 + \left(\frac{\Delta}{2eFd}\right)\cos\left(\frac{2\pi t}{\tau_B}\right) \tag{2.25}$$

This shows that the electron undergoes periodic motion in the momentum as well as real space

with a temporal period τ_B and spatial period L given by

$$\tau_B = h/eFd \tag{2.26}$$

$$L = \Delta/eFd \tag{2.27}$$

where Δ is the width of the miniband, and eFd is the WSL spacing, as described in the previous section.

One could also consider a tight-binding picture, where we look at the superlattice as an infinite number of quantum wells separated by barriers with a period d. The WSL eigenstates in this scheme are well-known

$$\chi_p^e(z) = \sum_n J_{n-p}(L/d) f^e(z - nd) \tag{2.28}$$

where J_p is a Bessel function of the first kind of order p and $f^e(z)$ is the electron wave function resulting from a single-site potential. One can then form an initial wavepacket using a superposition of these states, and calculate it's time evolution, as was done by Dignam et al.[23] This evolution takes the following form.

$$\Psi^{ni}(z;t) = \sum_p C_p e^{-ip\omega t} \sum_n J_{n-p}(L/d) f^e(z - nd) \tag{2.29}$$

$$\equiv \sum_n B_n(t) f^e(z - nd) \tag{2.30}$$

where the C_p are taken to be real, and $B_n(t)$ is the time-dependant amplitude for finding the electron in the nth well. Using the recursion relations and sum rules for Bessel functions, one can show that the expectation values of z and z^2 in $\Psi^{ni}(z;t)$ are found via[23]

$$\langle z \rangle = d \sum_p C_p^2 p + \cos(\omega t) L \sum_p C_{p-1} C_p \tag{2.31}$$

and

$$\left\langle z^2 \right\rangle = \left\langle z^2 \right\rangle_0 + \frac{L^2}{2} + d^2 \sum_p C_p^2 p^2 + \cos(\omega t)\, Ld \sum_p C_p C_{p-1}(2p-1) + \cos(\omega t)\, \frac{L^2}{2} \sum_p C_p C_{p-2} \tag{2.32}$$

where $\left\langle z^2 \right\rangle_0$ is the expectation value of z^2 in the state $f^e(z)$ localized at $z = 0$. It was found [23] that the motion of the wavepacket is periodic with the amplitude of oscillation given by

$$A_z \equiv L \left| \sum_p C_{p-1} C_p \right| \tag{2.33}$$

$$= L \left| \sum_n B_{n-1}(0)\, B_n(0) \right|, \tag{2.34}$$

which has an upper limit given by L.

If we choose the $C_p = J_{-p}(L/d)$, then we get that $B_n(t=0) = \delta_{n,0}$, which gives $A_z = 0$. This corresponds to a 'breathing mode', in which the wavepacket expands and contracts symmetrically. In general, one would not expect the wave packet to take one this form. The breathing mode and the semiclassical BO represent two extremes in the range of possible motions for this system.

For a finite superlattice consisting of N periods and miniband width Δ, the simple energy-dispersion relation given above shows that in the absence of an applied electric field, the energy levels will be unequally spaced. If an applied field strong enough that $NeFd > \Delta$ is applied, then one will obtain a WSL, which has equally spaced levels, separated by eFd. If one then excites this WSL by a pulsed laser whose spectrum encompasses more than one of the ladder's energy levels, one will excite a wavepacket made up of a superposition of various eigenstates. This wavepacket would be expected to undergo periodic oscillations. This is an extension of the concepts developed for the case of the coherent oscillations of an electronic wavepacket in an semiconductor double quantum well structure, as was investigated by Leo et al.[2] The periodic motion of the wavepacket in this case is, in general, the Bloch oscillations we have been looking for. These oscillations should be detectable by four-wave mixing experiments, just as in the case of the double quantum well. These experiments will be discussed in the next section.

2.4 Transient Degenerate Four-Wave Mixing Experiments

Transient FWM experiments are a powerful tool for the study of coherent effects in superconductors. The simplest setup for these experiments is shown in Figure 2-4. In this setup, referred to as a two-pulse self-diffraction geometry, two laser pulses with wave vectors $\mathbf{k}_1$ and $\mathbf{k}_2$ at times $t = 0$ and $t = \tau$, respectively, impinge upon the sample. The first laser pulse induces a first-order polarization in the sample. The second pulse interferes with this polarization to produce a carrier density grating in the direction $\mathbf{k}_2 - \mathbf{k}_1$. Due to nonlinear optical interaction, the electric field and linear polarization of the second laser pulse diffracts off of this grating in the phase-matched direction $2\mathbf{k}_2 - \mathbf{k}_1$. This creates a third-order polarization, which is the source of the measured FWM signal. The FWM signal can be measured time-integrated as a function of the time delay τ by using a slow photodetector. We can also time-resolve the FWM signal for each τ by using an up-conversion technique. The difference between DFWM and FWM is that the two laser pulses have the same central frequency in DFWM, whereas in FWM this is not the case.

In 1992, Feldmann et al.[3] performed DFWM experiments on a 91-period superlattice, consisting of 95 Å GaAs, and 15 Å $Al_{0.3}Ga_{0.7}As$ embedded in a p-i-n diode. At intermediate electric fields, a photocurrent spectra exhibit peaks corresponding to optical transitions of the WSL. In this regime, the heavy-hole states are already localized to a single well, whereas the electron states in the conduction band are still partially delocalized over several SL periods. This allows 'oblique' transitions to take place between a particular localized hole state, and a partially delocalized electron state, centered in a well n periods away. These transitions are illustrated in part (b) of Figure 2-5. The transitions are labelled as S_n. One should note that the peak measurements in (b) were made under the same conditions as the transient DFWM curves in (a).

In Figure 2-5 (a), the time-integrated DFWM signal is shown for several applied voltages at forward bias. The vertical arrow in (b) indicates the energy of the central frequency of the laser. At the highest voltage, 0.95 V, the decay of the signal is approximately exponential, and shows no extra features. In the intermediate voltages, however ($0.4 \rightarrow 0.7$ V), there is a pronounced modulation in the curve. The time duration T between the observed peaks decreases as the

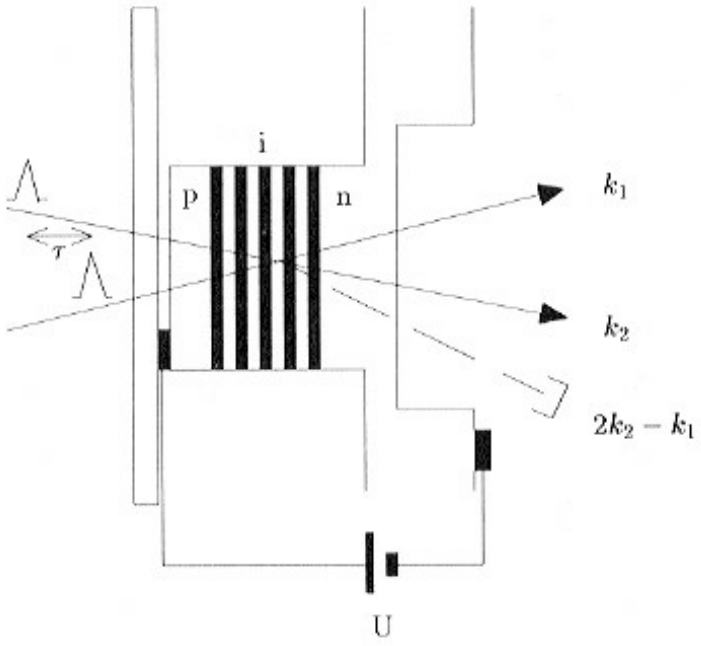

Figure 2-4: Schematic of a two-beam FWM experiment on an electrically biased superlattice. (from [19])

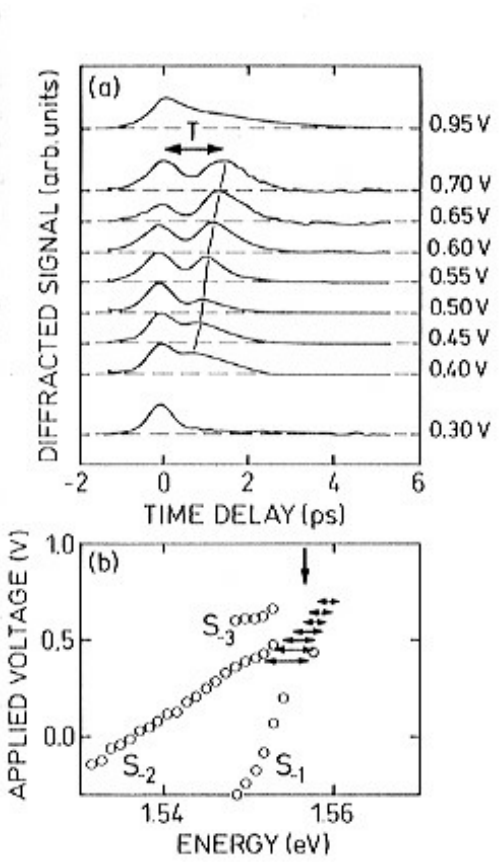

Figure 2-5: (a) DFWM signal versus time delay between the two laser pulses for several voltages in the WS ladder regime, showing modulations of the period T. (b) the peak positions of "oblique" transitions are plotted as circles versus the applied voltage. The energy intervals h/T, with T from (a), are shown as horizontal arrows.(from [3])

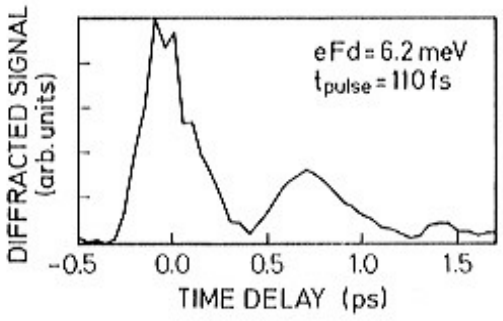

Figure 2-6: DFWM signal versus time delay for $eFd = 6.2$ meV using 110-fs laser pulses.(from [3])

field increases, and varies from 1.4 ps at 0.7 V to roughly 0.7 ps at 0.4 V. In order to find the source of these modulations, the energetic intervals h/T were drawn in Figure 2-5 (b). You can readily see for applied voltages less than 0.5 V that these intervals show good agreement with the energetic spacing eFd between the S_{-1} and S_{-2} transitions. For larger voltages, the h/T values decrease as expected from the tendency of the WS ladder spacings. This agreement of h/T with eFd indicates that the observed modulation times T are equivalent to the time periods τ_B expected for Bloch oscillations.

In Figure2-6, they show the time-integrated DFWM signal for a WSL spacing (eFd) of approximately 6.2 meV. This allows the spectrum of the laser pulse to encompass 5 WS transitions. AS you can see, there are three peaks on the curve, at 0, 0.7, and 1.4 ps. With the WSL spacing equal to 6.2 meV, the time period of Bloch oscillations, τ_B, is 0.67 ps, from equation 2.26. Again, there was found to be good agreement between the observed modulations in the DFWM signal, and the period of the Bloch oscillations in the superlattice.

Later that same year, Leo et al.[24] reported unambiguous evidence of Bloch oscillations, using a superlattice made up of 40 periods of 100 Å GaAs, and 17 Å $Al_{0.3}Ga_{0.7}As$. Transient FWM signals showed a periodic motion with a period strongly dependant on the electric field. They also noted that the peak spacing is inversely proportional to the electric field. This is consistent with the definition of the period for the Bloch oscillations2.26.

In Figure 2-7, the energies calculated for the oscillation periods observed in the FWM experiments are shown. The energy splitting shows the linear dependance on the electric field

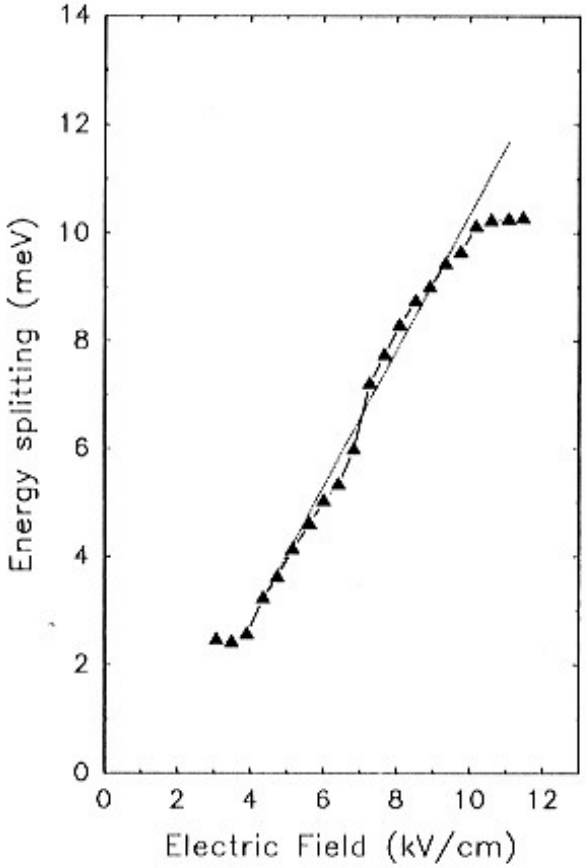

Figure 2-7: Energy splitting eFd calculated from the Bloch oscillation period using $eFd = h/\tau_B$. The dashed line indicates the expected slope for the Sl period of 117 . (from [24])

we expect from the WSL. The dashed line represents the slope expected based on the parameters of the SL. As you can see, there was good agreement between the expected results, and those obtained experimentally. This led them to conclude that the modulation of the FWM signals was caused by Bloch oscillations of the photoexcited electrons in the superlattice. They also found that the frequency of these Bloch oscillations could be tuned via the applied electric field.

In 1994, Dignam, Sipe and Shah[23] investigated theoretically the time evolution of electron and exciton wave packets in semiconductor superlattices when subjected to an electric field parallel to the plane of the superlattice layers. They were able to show that electron wave packets undergo Bloch oscillations, with the spacial amplitudes of these oscillations dependant

on the initial conditions. They also found that if they neglected the electron-hole Coulomb interaction in the field direction, the motion of the electron-hole separation ranged from a so-called 'breathing mode' to a semiclassical Bloch oscillation. When they included the Coulomb interaction into their formulation, they found that much of the character of the motion remained unaffected. However, the 'breathing mode' vanished, and there was an enhancement in the total oscillating dipole over a wide range of laser pulse parameters.

Also in 1994, P. Leisching et al. [25] did a detailed investigation of the coherent dynamics of excitonic wave packets in GaAs/Al_xGa_{1-x}As superlattices. They used a structure consisting of 35 periods of wells and barriers, with a constant well thickness of 17 , and an aluminum concentration of $x = 0.3$. They examined such things as the dependance of the FWM sinal on the applied electric field, the temperature dependance of Bloch oscillations, and the dependance of the oscillations on excitation conditions. They found that the oscillation period was highly dependant on the applied electric field, with a linear relationship at intermediate fields. Also, they were able to observe Bloch oscillations at temperatures of up to 200 K. By varying the excitation energy, they were able to create wave packets with a wide variety of shapes and oscillatory motions.

In 1995, Leisching et al. [26] showed that the nonlinear Coulomb interactions of Wannier Stark states in biased GaAs/Al_xGa_{1-x}As superlattices can be controlled by altering the external applied field .In 1998, Sudzius et al. [27] investigated the dependance of the dynamics of Bloch wave packets in superlattices on the optical excitation conditions. They found that for excitations well away from the center of the WSL, the wave packets perform harmonic oscillations; for excitations near the center of the WSL, the wave packets undergo a symmetric oscillation with virtually zero center-of-mass amplitude (a breathing mode).

In 2000, Löser et al.[28] investigated the influence of scattering and coherent plasmon coupling on the dynamics of Bloch-oscillating electrons in semiconductor superlattices. They demonstrated that the dynamics are highly influenced due to the scattering processes. They also found that for higher carrier densities, coupling to coherent plasmons leads to anharmonic Bloch oscillations since the static bias field in considerably altered by the oscillating carriers.

Chapter 3

Calculating the DFWM signal

In the previous chapter, we mentioned that the effect of FWM was to create a third-order polarization in the superlattice due to the interference between the second incident pulse, and the residual polarization left by the first one. This polarization propagates in the direction $2\mathbf{k}_2 - \mathbf{k}_1$. We refer to this polarization as $P_{inter}^{(22\bar{1})}$. The superscript $(22\bar{1})$ refers to the direction in which this third order polarization propagates, $\mathbf{k}_2 + \mathbf{k}_2 - \mathbf{k}_1$. In this chapter, we will derive the equations of motion which will enable us to calculate the FWM signal. We first develop the Hamiltonian for excitons in a superlattice under the influence of a static electric field. We do this using the variational method described by Dignam and Sipe[20] [29][30] Then, using the quasibosonic representation of Hawton and Nelson[9], we derive the exciton creation operator $B_\mu^\dagger$. We then, using an exciton basis in the long-wavelength limit, obtain the correlation functions necessary to calculate the DFWM signal to third order in the optical field.[31]

3.1 The Hamiltonian of excitons in a Superlattice

In the presence of a static electric field, the Hamiltonian for the exciton envelope function in a Type I or II superlattice can be written as[20][29]

$$H(z_e, z_h, r) = H_0(z_e, z_h, r) + U^e(z_e) + U^h(z_h) + eFz, \tag{3.1}$$

where $U^e(z_e)$ and $U^h(z_h)$ are the superlattice potentials for the electron and hole, respectively. $H_0(z_e, z_h, r)$ contains the kinetic and Coulomb energy terms, and is given by the following;

$$H_0(z_e, z_h, r) = \frac{-\hbar^2}{2\mu(z_e, z_h)} \frac{\partial}{\partial r} \frac{1}{r} \left[r \frac{\partial}{\partial r} \right] - \frac{\hbar^2}{2} \frac{\partial}{\partial z_e} \frac{1}{m^*_{ez}(z_e)} \frac{\partial}{\partial z_e} - \frac{\hbar^2}{2} \frac{\partial}{\partial z_h} \frac{1}{m^*_{hz}(z_h)} \frac{\partial}{\partial z_h} - \frac{e^2}{\epsilon \left(r^2 + z^2\right)^{\frac{1}{2}}} \tag{3.2}$$

In this equation, z_e and z_h represent the z coordinates of the electron and hole, respectively, $z \equiv z_e - z_h$, and r denotes the electron-hole separation in the transverse plane. The layer-dependant transverse electron-hole reduced effective mass, and is defined by $\mu(z_e, z_h)^{-1} \equiv m^*_{e\|}(z_e)^{-1} + m^*_{h\|}(z_h)^{-1}$, where $m^*_{e\|}(z_e)$ and $m^*_{h\|}(z_h)$ are the transverse effective masses for the electron and hole, respectively. The layer-dependant effective mass in the z-direction for the electron is $m^*_{ez}(z_e)$, and for the hole, $m^*_{hz}(z_h)$. The applied field strength is F, e is the charge on an electron, and ϵ represents the average dielectric constant of the superlattice structure.

The superlattice potentials $U^e(z_e)$ and $U^h(z_h)$ can be given in terms of the potentials of quantum wells, $V^e(z_e)$ and $V^h(z_h)$ by the following[29]

$$U^e(z_e) = \sum_m V^e(z_e - md), \text{ and} \tag{3.3}$$

$$U^h(z_h) = \begin{cases} \sum\limits_m V^h(z_h - md), \text{ for Type I superlattices} \\ \sum\limits_{m \neq 0} V^h[z_h - (1 - \frac{1}{2}|m|)md], \text{for Type II} \end{cases} \tag{3.4}$$

where

$$V^\sigma(z) = \begin{cases} -v_\sigma, \text{if } |z| < L_\sigma/2 \\ = 0 \text{ otherwise,} \end{cases} \tag{3.5}$$

where $\sigma = \{e, h\}$ denotes electron or hole, d is the period of the superlattice, L_e and L_h are the

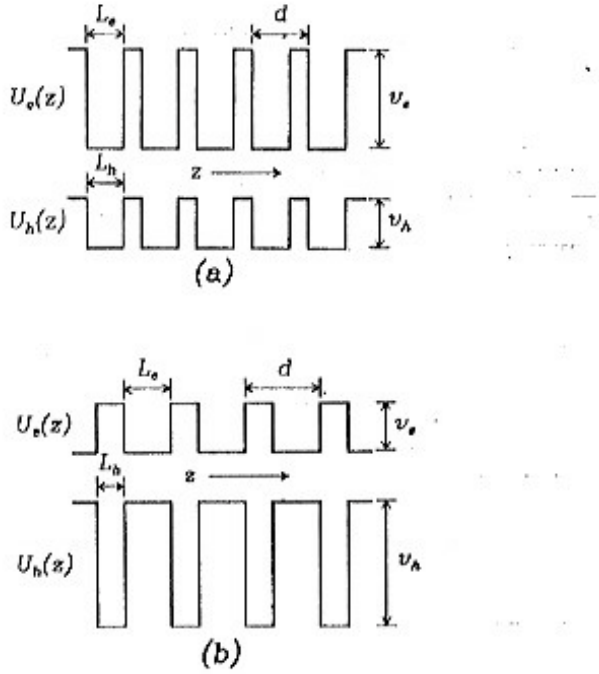

Figure 3-1: The periodic potentials for electrons $[U_e(z)]$ and holes $[U_h(z)]$ for (a) Type-1 superlattices and (b) Type-2 superlattices.(from [29])

thicknesses of the layers in which the electrons and holes are primarily confined, and v_e and v_h are the magnitude of the conduction and valence band discontinuities, respectively.

As you can see from Figure 3-1, the two types of superlattices differ in the alignment of the potential wells. In a Type I SL, the electron and hole potentials follow the same pattern of wells and barriers, and $L_e = L_h$. In the Type II SL, the electron well occupies the same physical location as the hole barrier, and vice versa. This leads to $L_e + L_h = d$, the period of the SL.

In order to calculate the eigenstates of H, we can make use of the translational symmetry of the superlattice structure[33]. In a way, this is similar to what is done in finding the eigenstates of a single particle in a periodic potential. In order to show this similarity in a simple way, we change the variables from z_e and z_h to the electron hole separation, $z = z_e - z_h$, along with $w = \alpha z_e + \beta z_h$, where w is the z component of the center of mass for the exciton. This is done by setting $\alpha = m^*_{e\perp}(z_e)/M$, and $\beta = m^*_{h\perp}(z_h)/M$, where M is simply the sum of the two effective masses, so that $\alpha + \beta = 1$. We now introduce a superlattice electron-hole translation

operator, T_m, which when used on a function of z_e and z_h, has the effect of shifting the two arguments by md, where m is an integer. Applying this to our new variables r, z, and w, we get the following:

$$T_m\varphi(r,z,w) = \varphi(r,z,w+md) \tag{3.6}$$

Since T_m commutes with H, we can use Bloch's theorem[33] and limit ourselves to eigenstates which satisfy

$$T_m\varphi(r,z,w) = e^{iqmd}\varphi(r,z,w), \tag{3.7}$$

where $|q| \leq \pi/d$. This will guarantee that these eigenstates, which we can label by q and a band index n, satisfy the following:

$$\widetilde{\psi}_n^q(r,z,w) = e^{iqw}u_n^q\left(r,z,w\right), \tag{3.8}$$

where $u_n^q\left(r,z,w\right)$ is periodic in w with a period equal to the superlattice period, d. The tilde on $\widetilde{\varphi}$ denotes that is a function of z and w, instead of z_e and z_h.

For fixed values of r, z, and w, $\widetilde{\varphi}_n^q(r,z,w)$ can be defined as a periodic function in reciprocal space. This allows us to introduce exciton Wannier functions, by using a Fourier expansion on $\widetilde{\varphi}_n^q(r,z,w)$, expressing it as a function of q, resulting in

$$\begin{aligned}
\widetilde{\psi}_n^q(r,z,w) &= \frac{1}{\sqrt{N}}\sum_m e^{iqmd}\widetilde{W}_n(r,z,w-md) &(3.9)\\
&= \frac{1}{\sqrt{N}}\sum_m e^{iqmd}W_n(r,z_e-md,z_h-md) &(3.10)
\end{aligned}$$

where in equation (3.10), we have switched back to using z_e and z_h as our variables. We can see from equation (3.9) that the exciton Wannier function, $\widetilde{W}_n(r,z,w)$, is quite similar to the single particle Wannier function, with the position of the center of mass of the exciton taking the place of the position of the particle. Also, the exciton function depends on the additional

coordinates of the internal motion of the exciton, z, and r.

We now wish to find expressions which will describe these exciton Wannier functions. In the same manner as the single particle in a periodic potential, we can utilize a tight-binding approximation by expanding the Wannier functions in a restricted basis. The basis which we will use are the eigenstates of the electric-field dependent two-well Hamiltonians, H_l, where l is an integer.[30]

$$H_l = H_0 + V_F^h(z_h) + V_F^e(z_e - s_l) \tag{3.11}$$

The position of the center of these wells are given by

$$s_l = \begin{cases} ld, \text{ for Type I SLs, or} \\ (1 - 1/2\,|l|)ld, \text{ for Type II SLs} \end{cases} \tag{3.12}$$

The potential wells are defined by the following:

$$V_F^\sigma(z) = \begin{cases} q_\sigma F L_\sigma/2, \text{ if } z < -L_\sigma/2, \\ -v_\sigma - q_\sigma F z, \text{ if } |z| < L_\sigma/2, \\ -q_\sigma F L_\sigma/2, \text{ if } z > L_\sigma/2. \end{cases} \tag{3.13}$$

The ground-state $\phi_l(r, z_e, z_h)$ of the two-well Hamiltonian H_l, is an exciton state. In this state, the hole is localized in the well at the origin and the electron is localized in the well at s_l, with 1s-like transverse motion.

We can now write the Hamiltonian in the form

$$H = H_l + \Delta_0^h(z_h) + \Delta_0^e(z_e) \tag{3.14}$$

where

$$\Delta_l^\sigma(z) = U^\sigma(z) - V_0^\sigma(z - s_l) - P_l^\sigma(z). \tag{3.15}$$

We now have to determine the ground states of the two-well Hamiltonians, H_l. These cannot be found analytically, however, they can be solved for variationally by using the 1s-like variational wave function[30]

$$\phi_l(r, z_e, z_h) = \left(\frac{2}{\pi}\right)^{1/2} \lambda f_l^e(z_e - s_i) f_l^h(z_h - s_j) \tag{3.16}$$

where λ is a variational parameter which depends upon $|S_i - S_j|$, and

$$f_l^\sigma(z) = \begin{cases} Ae^{\rho z}, \text{ if } z < -L_\sigma/2, \\ B\cos(kz), \text{ if } |z| < L_\sigma/2, \\ Ce^{-\tau z} \text{ if } z > L_\sigma/2, \end{cases} \tag{3.17}$$

A, B, and C are determined by requiring that $f_{ij}^\sigma(z)$ is a normalized function, and is also continuous at the layer boundaries. The value of the parameter k is set to be that of the lowest eigenstate of a single particle in a finite well in the absence of an electric field. ρ and τ can be determined due to the continuity of $[1/m_{\sigma z}^*(z)]\,(\partial/\partial z)\, f_l^\sigma(z)$ at the interfaces between the well layer and the adjacent barrier layers. [34] Since $f_l^\sigma(z)$ is a small quantity at all of the other interfaces, we can make the approximation that it's derivative is continuous there.

Thus, using this formulism, the eigenstates of the superlattice Hamiltonian are created via a tight binding of two-well exciton ground states. These states cover all possible electron-hole separations (l), centered on all possible sites.[30] This gives us the following equation:

$$\psi_n^q(r, z_e, z_h) = \frac{1}{\sqrt{N}} \sum_{l,m} e^{iqmd} b_l^n \phi_l(r, z_e - md, z_h - md), \tag{3.18}$$

where, by diagonalizing H in this nonorthonormal basis we can determine the b_l^n, which are the expansion coefficients found. This then reduces the problem to solving the generalized

eigenvalue equation

$$H_{jl}^{q} b_{l}^{n} = E_{n}^{q} A_{jl}^{q} b_{l}^{n} \tag{3.19}$$

where $A_{jl}^{q} = \left\langle \Phi_{j}^{q} \middle| \Phi_{l}^{q} \right\rangle$, the E_{n}^{q} are the exciton energy eigenvalues for the full superlattice, and

$$\begin{aligned} H_{jl}^{q} &= \left\langle \Phi_{j}^{q} \middle| H \left| \Phi_{l}^{q} \right\rangle \right. & (3.20) \\ &= E_{l}^{TW} A_{jl}^{q} + \sum_{m} e^{iqmd} \left\langle \Phi_{j}^{m} \middle| \Delta_{0}^{h} + \Delta_{l}^{e} \left| \Phi_{l}^{0} \right\rangle \right. & (3.21) \end{aligned}$$

where E_{l}^{TW} is the ground-state energy of the two-well Hamiltonian, H_{l}, and

$$\left\langle r, z_{e}, z_{h} \right| \left. \Phi_{l}^{q} \right\rangle = \frac{1}{\sqrt{N}} \sum_{l,m} e^{iqmd} \phi_{l}(r, z_{e} - md, z_{h} - md) \tag{3.22}$$

In equation (3.21), we have made the approximation that $\phi_{l}(r, z_{e}, z_{h})$ is a exact eigenstate of the two-well Hamiltonian, when, in fact, it is only a variational solution.

In practice, we use a finite number of two-well eigenstates, $\phi_{l}(r, z_{e}, z_{h})$, $(-l_{\max} \leq l \leq l_{\max})$, in order to calculate the various eigenstates and eigenvectors of the Hamiltonian. We choose the truncation point of this basis such that the calculated spectra remain basically unchanged by further increasing this basis size. This is possible due to the localization effect of the Wannier function.

3.2 Quasibosonic Representation

In this section, we will introduce the various the various operators used in the conversion from fermion to qboson space. These operators are used in the derivation of the correlation function describing DFWM in superlattices.

In a two-band model consisting of one conduction band and one valence band, the operator $\alpha_{\mathbf{k}}$ annihilates an electron with a wave vector $\mathbf{k}$ while $\beta_{\mathbf{k}}$ similarly destroys a hole. By combining these, we can create an operator which annihilates an electron-hole pair, with a center -of-mass

wave vector $\mathbf{K}$ and electron-hole relative wave vector $\mathbf{k}$.[6] This operator takes the form

$$b_{\mathbf{k},\mathbf{K}} = \beta_{-\mathbf{k}+\boldsymbol{\alpha}_h\mathbf{K}}\alpha_{\mathbf{k}+\boldsymbol{\alpha}_e\mathbf{K}} \tag{3.23}$$

We will use the collective indice $k_i = \{\mathbf{k}_i, \mathbf{K}_i\}$ to describe the state of the ith pair. The operators b_{k_i} and $b^\dagger_{k_i}$ thus annihilate and create, respectively, an electron and hole with a center-of-mass wave vector $\mathbf{K}_i$ and a relative wave vector $\mathbf{k}_i$.

We are assuming the these operators are acting in a system which contains an equal number of electrons and holes. A fermionic state which satisfies this condition does not make any allowance for pairing. The state containing two electron hole pairs with wave vectors $(\mathbf{k}_1, -\mathbf{k}_1; \mathbf{k}_2, -\mathbf{k}_2)$ is equivalent to one with wave vectors $(\mathbf{k}_1, -\mathbf{k}_2; \mathbf{k}_2, -\mathbf{k}_1)$, since the same two electrons and holes are present. However, if we look at these two pairs as excitons, we can readily see that these are two different states, where only the first has two pairs each with zero center-of-mass wave vectors. There is a 1-to-n! correspondence between fermion space, and the equivalent boson space, where there are n! nonequivalent permutations of the electrons for fixed holes.

Since the excitons we are concerned with are not ideal bosons, we will call the space of paired electrons and holes pair space, or qboson space. In this new space, states are symmetric under the exchange of pairs, however, they are not necessarily antisymmetric under the exchange of individual electrons or holes. The fermion exchange energy is included in the energies of individual excitons and in the exciton-exciton interaction energies.

In order to transform the fermionic pair operators b_{k_i} and $b^\dagger_{k_i}$ into their qbosonic pair equivalents, B_{k_i} and $B^\dagger_{k_i}$, Usui's transformation[32] will be used, as described in Hawton and Nelson.[9] The exciton operators $B^\dagger_{n,\mathbf{K}}$ can be introduced as a linear combination of the qbosonic ones as follows

$$B^\dagger_{n,\mathbf{K}} = \sum_{\mathbf{k}} \psi_{n,\mathbf{k}} B^\dagger_{\mathbf{k},\mathbf{K}} \tag{3.24}$$

where $\psi_{n,\mathbf{k}}$ is the k-space representation of our basis, and periodic boundary conditions have been used. If we multiply both sides of Equation (3.24) by $\psi_{n,\mathbf{k}'}$, sum over n, and then apply

the completeness of the basis, we get the inverse transformation as seen here

$$B^{\dagger}_{\mathbf{k},\mathbf{K}} = \sum_{n} \psi^{*}_{n,\mathbf{k}} B^{\dagger}_{n,\mathbf{K}}$$

While this transformation affects the relative motion of the electron and hole, the center-of-mass motion remains the same. We can define a second collective indice $\nu_i = \{n_i, \mathbf{K}_i\}$, which allows us to write the exciton creation operator as $B^{\dagger}_{\nu}$. The commutators of exciton annihilation and creation operators become, after some algebra,[9]

$$\left[B_{\nu_1}, B^{\dagger}_{\nu_2}\right] = \delta_{\nu_1,\nu_2} - 2 \sum_{m_1,m_2} \chi^{n_1,n_2,\mathbf{K}_1-\mathbf{K}_2}_{m_1,m_2} B^{\dagger}_{\mu_2} B_{\mu_1} \tag{3.25}$$

where $\mu_i = \{m_i, \mathbf{K}_i\}$ and

$$\chi^{n_1,n_2,\mathbf{Q}}_{m_1,m_2} = \frac{1}{2}\sum_{\mathbf{k}} \psi^{*}_{n_1,\mathbf{k}} \psi_{n_2,\mathbf{k}+\boldsymbol{\alpha}_h\mathbf{Q}} \psi^{*}_{m_2,\mathbf{k}+\boldsymbol{\alpha}_h\mathbf{Q}} \psi_{m_1,\mathbf{k}} + \psi^{*}_{n_1,\mathbf{k}} \psi_{n_2,\mathbf{k}-\boldsymbol{\alpha}_e\mathbf{Q}} \psi^{*}_{m_2,\mathbf{k}-\boldsymbol{\alpha}_e\mathbf{Q}} \psi_{m_1,\mathbf{k}} \tag{3.26}$$

These χ parameters describe phase-space filling, and can be calculated for any given exciton basis. The parameter $\chi^{n_1,n_1,0}_{n_1,n_1}$ is the average probability for the occurrence of any given pair. If $\chi = 0$, then the excitons are bosons.

3.3 Calculating $\chi^{\mu,\mu'}_{\mu'',\mu'''}$

In the previous section, we introduced the parameter $\chi^{n_1,n_2}_{m_1,m_2}$, which describes phase-space filling. In this section, we will derive expressions which allow us to calculate this parameter for the 1s excitons we are concerned with. We have set the value of $\mathbf{Q}$ equal to zero.

We have that

$$\psi^{\mu,0}\left(z_e, z_h, \boldsymbol{\rho}\right) = \sum_{n,m,\mathbf{k}} \psi^{\mu}_{n,m}\left(\mathbf{k}\right) \phi_{n,m,\mathbf{k},0}\left(r_e, r_h\right) \tag{3.27}$$

where

$$\phi_{n,m,\mathbf{k},0}\left(r_e, r_h\right) = e^{i\mathbf{k}\cdot\boldsymbol{\rho}} \chi^{e}_{n+m}(z_e) \chi^{h}_{n}(z_h) \tag{3.28}$$

For a 1s exciton, the wavefunction, using a two-well basis is given by[30]

$$\psi^{\mu,0}\left(z_e, z_h, \boldsymbol{\rho}\right) = \frac{1}{\sqrt{N_z}} \frac{1}{\sqrt{A}} \sum_{n,l} D_l^{\mu} f_n\left(z_h - nd\right) f_e\left(z_e - \left(n+l\right) d\right) \phi_l\left(\boldsymbol{\rho}\right) \tag{3.29}$$

where $f(z)$ is given by equation (3.17) above. The D_l^{μ} are expansion coefficients found by diagonalizing the exciton Hamiltonian in the two-well basis.[35] What we need to derive in this section is the relationship between the f functions in (3.29) and the χ functions in (3.28). This is possible if we make one of two assumptions: (1) χ is calculated in the nearest-neighbor tight-binding approximation, with localized states f, or (2) the f functions are the exact Wannier functions. Since we are already using a tight-binding approximation in our calculation of the Hamiltonian, it makes sense to continue using it here. Also, this allows us to take advantage of certain properties of Bessel functions. This leads us to write that

$$\chi_m^{\sigma}(z) = \sum_p J_{p-m}(\theta_{\sigma}) f_{\sigma}(z - pd) \tag{3.30}$$

Here, $\theta_e = \dfrac{\Delta_e}{2eFd}, \theta_h = \dfrac{-\Delta_h}{2eFd}$, where Δ_e and Δ_h are the electron and hole bandwidths, respectively. Now, we know that[36]

$$\sum_p J_{p-m}(\theta) J_{p-m'}(\theta) = \delta_{m,m'} \tag{3.31}$$

and thus

$$f_{\sigma}(z - pd) = \sum_m J_{p-m}(\theta_{\sigma}) \chi_m^{\sigma}(z) \tag{3.32}$$

Substituting this last equation back into (3.30), we get

$$\chi_m^{\sigma}(z) = \sum_p J_{p-m}(\theta_{\sigma}) \sum_{m'} J_{p-m'}(\theta_{\sigma}) \chi_{m'}^{\sigma}(z) \tag{3.33}$$

applying equation (3.31) to this leaves us with

$$\chi_m^\sigma(z) = \sum_{m'} \delta_{m,m'} \chi_{m'}^\sigma(z) \tag{3.34}$$

$$= \chi_m^\sigma(z) \tag{3.35}$$

indicating that our relationship between f and χ is correct. Now, taking equation (3.32), and using it in equation (3.29), we get the following

$$\psi^{\mu,0}(z_e, z_h, \boldsymbol{\rho}) = \frac{1}{\sqrt{N_z}} \frac{1}{\sqrt{A}} \sum_{n,l} D_l^\mu \phi_l(\boldsymbol{\rho}) \sum_{m,m'} J_{n-m}(\theta_h) J_{n+l-m}(\theta_e) \chi_m^h(z_h) \chi_{m'}^e(z_e) \tag{3.36}$$

Another convenient property of the Bessel functions is that[36]

$$\sum_n J_{n-m}(\theta_h) J_{n+l-m'}(\theta_e) = J_{l+m-m'}(\theta) \tag{3.37a}$$

Now, using equation (3.37a) in (3.36), we obtain

$$\psi^{\mu,0}(z_e, z_h, \boldsymbol{\rho}) = \frac{1}{\sqrt{N_z}} \frac{1}{\sqrt{A}} \sum_l D_l^\mu \phi_l(\boldsymbol{\rho}) \sum_{m,m'} J_{l+m-m'}(\theta) \chi_m^h(z_h) \chi_{m'}^e(z_e) \tag{3.38}$$

$$= \frac{1}{\sqrt{N_z}} \frac{1}{\sqrt{A}} \sum_l D_l^\mu \phi_l(\boldsymbol{\rho}) \sum_{n,m} J_{l-m}(\theta) \chi_n^h(z_h) \chi_{n+m}^e(z_e) \tag{3.39}$$

Now we will turn our attention to $\phi_l(\boldsymbol{\rho})$. If we let

$$\phi_l(\boldsymbol{\rho}) = \sum_{\mathbf{k}} \Phi_l(\mathbf{k}) e^{i(\mathbf{k}\cdot\boldsymbol{\rho})} \tag{3.40}$$

$$\Phi_l(\mathbf{k}) = \frac{1}{A} \int d^2\rho \phi_l(\boldsymbol{\rho}) e^{i(\mathbf{k}\cdot\boldsymbol{\rho})} \tag{3.41}$$

Now, in the 1s basis, we can write $\phi_l(\boldsymbol{\rho})$ as

$$\phi_l(\boldsymbol{\rho}) = \sqrt{\frac{2}{\pi}} \lambda_l e^{-\lambda_l \rho} \tag{3.42}$$

Substituting this last expression into equation (3.41), we get

$$\Phi_l(\mathbf{k}) = \frac{1}{A}\sqrt{\frac{2}{\pi}}\int d^2\rho\lambda_l e^{-\lambda_l\rho}e^{i(\mathbf{k}\cdot\boldsymbol{\rho})} \tag{3.43}$$

$$= \frac{1}{A}\sqrt{\frac{2}{\pi}}\lambda_l\int_0^\infty d\rho\cdot\rho e^{-\lambda_l\rho}\int_0^{2\pi} e^{i(k\cdot\boldsymbol{\rho})\cos\phi} \tag{3.44}$$

where this last equation is now independent of the direction of $\mathbf{k}$. Now we know that $\int_0^{2\pi} e^{i(k\cdot\boldsymbol{\rho})\cos\phi} = 2\pi J_0(k\rho)$. Using this in our latest equation gives us

$$\Phi_l(\mathbf{k}) = \frac{2\pi}{A}\sqrt{\frac{2}{\pi}}\lambda_l\int_0^\infty d\rho\cdot\rho e^{-\lambda_l\rho}J_0(k\rho) \tag{3.45}$$

Now, from [36], we get the following:

$$\int_0^\infty dx\cdot xe^{-ax}J_0(bx) = \frac{2a\cdot 2b\cdot\Gamma\left(\frac{3}{2}\right)}{\sqrt{\pi}\left(a^2+b^2\right)^{3/2}} \tag{3.46}$$

using this in equation (3.45) gives us

$$\Phi_l(\mathbf{k}) = \frac{2\pi}{A}\sqrt{\frac{2}{\pi}}\lambda_l\frac{2\lambda_l\cdot\Gamma\left(\frac{3}{2}\right)}{\sqrt{\pi}\left(\lambda_l^2+k^2\right)^{3/2}} \tag{3.47}$$

$$= \frac{2\pi}{A}\sqrt{\frac{2}{\pi}}\lambda_l\frac{\lambda_l^2}{\left(\lambda_l^2+k^2\right)^{3/2}} \tag{3.48}$$

since $\Gamma\left(\frac{3}{2}\right) = \sqrt{\pi}/2$.

Now, if we take equation (3.39) and apply equation (3.40),we get

$$\psi^{\mu,0}(z_e,z_h,\boldsymbol{\rho}) = \frac{1}{\sqrt{N_z}}\frac{1}{\sqrt{A}}\sum_l D_l^\mu\phi_l(\boldsymbol{\rho})\sum_{n,m,\mathbf{k}}\Phi_l(\mathbf{k})\cdot A\cdot J_{l-m}(\theta)\cdot\frac{e^{i(\mathbf{k}\cdot\boldsymbol{\rho})}}{A}\chi_n^h(z_h)\chi_{n+m}^e(z_e) \tag{3.49}$$

If we compare this equation to (3.27), we can readily see that

$$\psi_{n,m}^\mu(\mathbf{k}) = \frac{1}{\sqrt{N_z}}\sum_l D_l^\mu\Phi_l(\mathbf{k})\sqrt{A}J_{l-m}(\theta) \tag{3.50}$$

applying equation (3.48)

$$\psi^{\mu}_{n,m}(\mathbf{k}) = \frac{2\sqrt{2\pi}}{\sqrt{A}\sqrt{N_z}} \sum_{l} \frac{D^{\mu}_{l} J_{l-m}(\theta) \lambda_l^2}{\left(\lambda_l^2 + k^2\right)^{3/2}} \tag{3.51}$$

$$= \psi^{\mu}_{m}(\mathbf{k}) \tag{3.52}$$

The reason we are able to drop the subscript n is because this equation has no dependance on n anywhere. Now that we have an expression for $\psi^{\mu}_{m}(\mathbf{k})$, we can get down to determining $\chi^{\mu,\mu'}_{\mu'',\mu'''}$. Rewriting equation (3.26) to use our notation here gives us the following

$$\chi^{\mu,\mu'}_{\mu'',\mu'''} = \frac{1}{2} \sum_{m,m'} \sum_{n,n'} \sum_{\mathbf{k}} \psi^{\mu *}_{m}(\mathbf{k}) \psi^{\mu'}_{m'}(\mathbf{k}) \psi^{\mu'' *}_{m'}(\mathbf{k}) \psi^{\mu'''}_{m}(\mathbf{k}) \left[\delta_{n',n} + \delta_{m',m+n-n'}\right] \tag{3.53}$$

$$= \frac{1}{2} N_z \sum_{m,m'} \sum_{\mathbf{k}} \psi^{\mu *}_{m}(\mathbf{k}) \psi^{\mu'}_{m'}(\mathbf{k}) \psi^{\mu'' *}_{m'}(\mathbf{k}) \psi^{\mu'''}_{m}(\mathbf{k}) \tag{3.54}$$

Now using equation (3.51) on each pair of ψ with the same m subscript gives us the following

$$\sum_{m} \psi^{\mu *}_{m}(\mathbf{k}) \psi^{\mu'''}_{m}(\mathbf{k}) = \frac{8\pi}{AN_z} \sum_{l,l'} \frac{D^{\mu *}_{l} D^{\mu'''}_{l'} \lambda_l^2 \lambda_{l'}^2}{\left(\lambda_l^2 + k^2\right)^{3/2} \left(\lambda_{l'}^2 + k^2\right)^{3/2}} \sum_{m} J_{l-m}(\theta) J_{l'-m}(\theta) \tag{3.55}$$

Applying equation (3.31) to this yields a $\delta_{l,l'}$ for the two Bessel functions, and thus

$$\sum_{m} \psi^{\mu *}_{m}(\mathbf{k}) \psi^{\mu'''}_{m}(\mathbf{k}) = \frac{8\pi}{AN_z} \sum_{l} \frac{D^{\mu *}_{l} D^{\mu'''}_{l} \lambda_l^4}{\left(\lambda_l^2 + k^2\right)^3} \tag{3.56}$$

Applying this to both the m terms and m' terms in equation (3.54), we get that

$$\chi^{\mu,\mu'}_{\mu'',\mu'''} = \frac{(8\pi)^2}{A^2 N_z} \sum_{l,l'} \sum_{\mathbf{k}} \frac{D^{\mu *}_{l} D^{\mu'''}_{l} \lambda_l^4}{\left(\lambda_l^2 + k^2\right)^3} \frac{D^{\mu'}_{l'} D^{\mu'' *}_{l'} \lambda_{l'}^4}{\left(\lambda_{l'}^2 + k^2\right)^3} \tag{3.57}$$

Now we can write that

$$\sum_{\mathbf{k}} f(\mathbf{k}) = \frac{A}{(2\pi)^2} \int_0^{\infty} d\mathbf{k} \cdot \mathbf{k} \int_0^{2\pi} d\phi f(\mathbf{k}) \tag{3.58}$$

$$= \frac{A}{2\pi} \int_0^{\infty} d\mathbf{k} \cdot \mathbf{k} f(\mathbf{k}) \tag{3.59}$$

$$= \frac{A}{4\pi} \int_0^{\infty} d\mathbf{x} f(\sqrt{\mathbf{x}}) \tag{3.60}$$

applying this to equation (3.57) gives that

$$\sum_{\mathbf{k}} \frac{\lambda_l^4}{\left(\lambda_l^2+k^2\right)^3}\frac{\lambda_{l'}^4}{\left(\lambda_{l'}^2+k^2\right)^3} = \frac{A\lambda_l^4\lambda_{l'}^4}{4\pi}\int_0^\infty \frac{dx}{\left(\lambda_l^2+k^2\right)^3\left(\lambda_{l'}^2+k^2\right)^3} \tag{3.61}$$

If we denote

$$F\left(\lambda_\ell,\lambda_{\ell'}\right) = \frac{\lambda_\ell^4\lambda_{\ell'}^4}{a_0^2}\int_0^\infty \frac{dx}{\left(\lambda_\ell^2+x\right)^3\left(\lambda_{\ell'}^2+x\right)^3} \tag{3.62}$$

This integral is analytic, and can be evaluated by the following expression

$$F\left(\lambda_\ell,\lambda_{\ell'}\right) = \frac{1}{2a_0^2}\frac{\lambda_\ell^8-8\lambda_\ell^6\lambda_{\ell'}^2+24\lambda_\ell^4\lambda_{\ell'}^4\ln\lambda_\ell-24\lambda_\ell^4\lambda_{\ell'}^4\ln\lambda_{\ell'}+8\lambda_\ell^2\lambda_{\ell'}^6-\lambda_{\ell'}^8}{\left(3\lambda_\ell^2\lambda_{\ell'}^4-3\lambda_\ell^4\lambda_{\ell'}^2-\lambda_\ell^6+\lambda_{\ell'}^6\right)\left(\lambda_\ell^4-\lambda_\ell^2\lambda_{\ell'}^2+\lambda_{\ell'}^4\right)} \tag{3.63}$$

using our definition for$F\left(\lambda_\ell,\lambda_{\ell'}\right)$ in equation (3.57), we get that

$$\chi^{\mu,\mu'}_{\mu'',\mu'''} = \frac{16\pi}{AN_z}\sum_{l,l'} D_l^{\mu *} D_l^{\mu'''} D_{l'}^{\mu'} D_{l'}^{\mu''*}\cdot F\left(\lambda_\ell,\lambda_{\ell'}\right) \tag{3.64}$$

3.4 The Equations of motion for $B_\mu^\dagger$

In this section, we will derive the equations of motion needed to calculate the expectation value of the exciton creation operator $B_\mu^\dagger$ to third order. We do this by first obtaining the Hamiltonian for excitons in a superlattice under the influence of a static electric field. We then derive the Heisenberg equations for the creation and annihilation operators of excitons. With these, we can create the equations of motion for the various functions needed to obtain the DFWM polarization to third order in the optical field.

We can write the total energy of a system of charges as the sum of the kinetic energies of the various charges, plus the electric and magnetic energy stored in the medium. We will only include those electrons found in the highest valence miniband, and the lowest conduction miniband associated with the superlattice. The effects of the electrons present in all other bands can be accounted for via external fields, as well as an external potential, $U^{ext}\left(\mathbf{r}\right)$. We can treat the electric field effects caused by these other charges by introducing a dielectric constant, ε. This leads to the electric field, $E\left(\mathbf{r},t\right)$, arising from the fields from the system

electrons, as well as externally applied fields. Since we have a neutral system, we can apply the Power-Zienau-Woolley transformation to the minimal coupling Hamiltonian. This gives us the following equation for our Hamiltonian:

$$\begin{aligned} H^T &= \sum_\alpha \frac{1}{2} m_\alpha \mathbf{v}_\alpha^2 + U^{ext}(\mathbf{r}_\alpha) + \sum_\alpha V_\alpha^{self} + \sum_{\alpha \neq \beta} \frac{q_\alpha q_\beta}{8\pi\varepsilon |\mathbf{r}_\alpha - \mathbf{r}_\beta|} \\ &\quad + \int d^3r \left[\frac{1}{2}\varepsilon \mathbf{E}_\perp(\mathbf{r},t) \cdot \mathbf{E}_\perp(\mathbf{r},t) + \frac{1}{2\mu_0} \mathbf{B}(\mathbf{r},t) \cdot \mathbf{B}(\mathbf{r},t) \right], \end{aligned} \tag{3.65}$$

where α labels the electron which has mass m_α, velocity $\mathbf{v}_\alpha^2$, charge q_α and is found at position $\mathbf{r}_\alpha$. V_α^{self} describes the Coulomb self-energy associated with the α^{th} charge, $\mathbf{E}_\perp(\mathbf{r},t)$ is the transverse component of the electric field $\mathbf{E}(\mathbf{r},t)$, and $\mathbf{B}(\mathbf{r},t)$ is the total magnetic field. If we neglect the effects caused by the magnetic field, the canonical momentum of the electron in the system will be given by $\mathbf{p}_\alpha = m_\alpha \mathbf{v}_\alpha$. Also, we can derive the Coulomb and self energies from a volume integral of the total longitudinal electric field as [31]

$$\int d^3r \frac{1}{2}\varepsilon \mathbf{E}_\parallel(\mathbf{r},t) \cdot \mathbf{E}_\parallel(\mathbf{r},t) = \sum_\alpha V_\alpha^{self} + \sum_{\alpha \neq \beta} \frac{q_\alpha q_\beta}{8\pi\varepsilon |\mathbf{r}_\alpha - \mathbf{r}_\beta|}. \tag{3.66}$$

Making this substitution into the Hamiltonian, equation (3.65) we get the following equation

$$H^T = \sum_\alpha \frac{\mathbf{p}_\alpha^2}{2m_\alpha} + U^{ext}(\mathbf{r}_\alpha) + \int d^3r \frac{1}{2}\varepsilon \mathbf{E}(\mathbf{r},t) \cdot \mathbf{E}(\mathbf{r},t). \tag{3.67}$$

This Hamiltonian is applicable to any semiconductor, where only the conductance and valence band electrons are being considered. We will use this as our starting point for determining the form of the Hamiltonian for the excitons in a biased semiconductor superlattice. If we use the envelope function approximation on the Hamiltonian, we arrive at the following Hamiltonian for the electron envelope function.

$$H = \sum_\alpha H_\alpha^o + \int d^3r \frac{1}{2}\varepsilon \mathbf{E}(\mathbf{r},t) \cdot \mathbf{E}(\mathbf{r},t), \tag{3.68}$$

H_α^o is the single electron Hamiltonian in the envelope function approximation for a biased

superlattice. In this case, this includes the potential arising from the applied along-axis external electric field, E_{dc}^{ext}, as well as those due to band-edge discontinuities.

Now that we know what H_α^o includes, can turn our attention to the remaining term of the equation, and determine the form of $\mathbf{E}$. This can be written as the sum of the field created by the electrons and holes, $\mathbf{E}^{int}$, and the ac potion of the externally applied field, $\mathbf{E}_{ac}^{ext}$.

$$\mathbf{E}(\mathbf{r},\mathbf{t}) = \mathbf{E}_{ac}^{ext}(\mathbf{r},t) + \mathbf{E}^{int}(\mathbf{r},t).$$

Our external ac field consists of optical and terahertz parts, i.e.

$$\mathbf{E}_{ac}^{ext}(\mathbf{r},t) = \mathbf{E}_{opt}^{ext}(\mathbf{r},t) + \mathbf{E}_{THz}^{ext}(\mathbf{r},t). \tag{3.69}$$

This external ac field does not include the static external bias field, which is included into the energy associated with H_α^o. For a neutral system, the field generated by the electrons and holes, $\mathbf{E}^{int}$ can be written as

$$\mathbf{E}^{int} = -\frac{\mathbf{P}^{int}(\mathbf{r},t)}{\varepsilon},$$

In this equation, $\mathbf{P}^{int}$ is the polarization created by the electrons and holes making up the system. By substituting these into our Hamiltonian, (3.68), we get the following

$$H = \sum_\alpha H_\alpha^o - \int d^3r \mathbf{E}^{ext}(\mathbf{r},t)\cdot\mathbf{P}^{int}(\mathbf{r},t) + \frac{1}{2\varepsilon}\int d^3r \mathbf{P}^{int}(\mathbf{r},t)\cdot\mathbf{P}^{int}(\mathbf{r},t). \tag{3.70}$$

In (3.70), the second term deals with the interaction between the carriers and the external fields, while the third term contains the electron-electron Coulomb interactions, which arise from the longitudinal portion of the polarization. The third term also includes interactions interaction which arise from the transverse portion of the induced polarization, which are usually neglected, but in this system play a vital role.

It is difficult to calculate $\mathbf{P}^{int}(\mathbf{r},t)$ exactly; therefore, we will look for an approximation which is suitable to our needs. In our approximation, there are two key factors which we must be sure are included. The intra-exciton Coulomb interaction between the electron and the

hole must be included. Secondly, the interexciton interactions must be included as well. In DFWM experiments, the exciton-exciton interactions are not considered to be of import. The wavelengths of the optical fields are quite large relative to the size of an exciton, thus it is to be expected that variations in the polarization will occur on scales much larger than the exciton Bohr radius. This allows us to treat the polarization in the dipole approximation.

We can now create our exciton Hamiltonian from equation (3.70) via the following changes. We will first pair up each electron with a hole, and label these pairs by γ. Since we are dealing with a neutral system, there are an equal number of each, i.e. no unpaired charges will remain. From the last term, we extract the parts which contain the interaction between the electron and hole within each pair (i.e. the intraexciton interaction), and denote this by V_γ. The remainder of the polarization can be replaced by it's dipole approximation, which we will call $\mathbf{P}(\mathbf{r},t)$. This gives us the following[31]

$$H = \sum_\gamma H_\gamma^{EX} - \int d^3r \mathbf{E}^{ext}(\mathbf{r},t)\cdot\mathbf{P}(\mathbf{r},t) + \frac{1}{2\varepsilon}\int d^3r \mathbf{P}(\mathbf{r},t)\cdot\mathbf{P}(\mathbf{r},t), \tag{3.71}$$

where $\sum_\gamma \left[H_\gamma^{EX} - V_\gamma\right] \equiv \sum_\alpha H_\alpha^o$. The single exciton Hamiltonian, H_γ^{EX} is the one considered by Dignam and Sipe[20][29]

In the interpretation of DFWM results, we are required to consider fields which have definite wave vectors, such as $2\mathbf{K}_2 - \mathbf{K}_1$, In becomes more convenient to rewrite the Hamiltonian above in $\mathbf{K}$ -space, via the use of Fourier transforms defined by

$$f(\mathbf{R},t) = \sum_{\mathbf{K}} f_{\mathbf{K}}(t)\, e^{i\mathbf{K}\cdot\mathbf{R}}. \tag{3.72a}$$

Here we are using the upper case $\mathbf{K}$ and $\mathbf{R}$ since these refer to the center of mass motion of the exciton, and it is this motion which couples to the $\mathbf{K}^{th}$ Fourier component of the field, and not the motions associated with the individual carriers. For a superlattice with volume V, the inverse Fourier transform is given by

$$f_{\mathbf{K}}(t) = \frac{1}{V}\int d^3R f(\mathbf{R},t)\, e^{-i\mathbf{K}\cdot\mathbf{R}} \tag{3.73}$$

where $f_{-\mathbf{K}}(t) = f^*_{\mathbf{K}}(t)$ for real $f(\mathbf{R}, t)$. Applying these transforms to our Hamiltonian, (3.71) gives us

$$H = H_0^{EX} + V\sum_{\mathbf{K}}\left(-\mathbf{E}^{ext}_{-\mathbf{K}}\cdot\mathbf{P}_{\mathbf{K}} + \frac{1}{2\varepsilon}\mathbf{P}_{-\mathbf{K}}\cdot\mathbf{P}_{\mathbf{K}}\right). \tag{3.74}$$

As has been done in previous work on this subject[29][30], we can use an exciton basis. The basis states, denoted by $\psi_{\mu,\mathbf{K}}(\mathbf{r},\mathbf{R})$, are the excitonic states after being subjected to the external dc electric field, E^{ext}_{dc}. Here, $\mathbf{r}$ describes the relative separation of the electron hole pair, $\mathbf{r}_e - \mathbf{r}_h$, and μ represents the quantum numbers of the internal motion associated with the exciton. These quantum numbers describe the average electron-hole separation and the in-plane hydrogenic state of the two-dimensional exciton. In the dipole approximation, the second quantized macroscopic polarization operator is given by

$$\mathbf{P}_{\mathbf{K}}(t) = \sum_{\mu}\left(\mathbf{M}_{\mu,\mathbf{K}}B^{\dagger}_{\mu,\mathbf{K}} + \mathbf{M}^{*}_{\mu,\mathbf{K}}B_{\mu,\mathbf{K}}\right) + \sum_{\mu,\mu',\mathbf{K}'}\mathbf{G}_{\mu,\mathbf{K}-\mathbf{K}';\mu',\mathbf{K}'}B^{\dagger}_{\mu,\mathbf{K}-\mathbf{K}'}B_{\mu',-\mathbf{K}'} \tag{3.75}$$

where

$$\mathbf{M}^{\mathbf{K}}_{\mu,\mathbf{K}'} = \mathbf{M}_o\delta_{\mathbf{K},\mathbf{K}'}\int d^3\mathbf{r}\psi_{\mu,\mathbf{K}}(\mathbf{r};\mathbf{r}) \tag{3.76}$$

with $\mathbf{M}_o = \frac{i\hbar e\mathbf{p}_{cv}}{m_o E_{gap}}$ is the bulk interband dipole matrix element. $\mathbf{G}_{\mu,\mathbf{K}-\mathbf{K}';\mu',\mathbf{K}'}$ represents the expectation value of the exciton dipole operator, and is given by

$$\mathbf{G}_{\mu,\mathbf{K}-\mathbf{K}';\mu',\mathbf{K}'} = e\int d^3r\int d^3R\psi_{\mu,\mathbf{K}-\mathbf{K}'}(\mathbf{r},\mathbf{R})\,\mathbf{r}\psi^{*}_{\mu',\mathbf{K}'}(\mathbf{r},\mathbf{R})\,e^{-i\mathbf{K}\cdot\mathbf{R}}. \tag{3.77}$$

These three quantities are all derived in the Appendix of Hawton and Dignam [31]. As in the previous section dealing with $X^{\mu,\mu'}_{\mu'',\mu'''}$, we are only considering $1s$ excitons here.

In equation (3.75), the first term is the interband polarization energy describing the creation and annihilation of the excitons. It is at optical frequencies, and operates parallel to the exciting electric field with wave vector $\mathbf{K}_1$ or $\mathbf{K}_2$ (i.e. in parallel with one of the laser pulses) and thus is transverse. The second term of this equation is the intraband polarization operator. The THz part of this term describes the correlations which exist between the various WSL states,

while the dc part represents the static excitonic dipole moment. The intraband polarization is parallel to the z-axis, with wave vectors such as $\mathbf{K}_2 - \mathbf{K}_1$. This implies that the intraband polarization has both a transverse and a longitudinal component.

Since the wavevectors we are interested in in these experiments are small, we can write $\mathbf{E}_{\mathbf{K}}$, the $\mathbf{K}^{th}$ component of the total electric field operator as

$$\mathbf{E}_{\mathbf{K}} = \mathbf{E}_{\mathbf{K}}^{ext} - \frac{1}{\varepsilon}\mathbf{P}_{\mathbf{K}}. \tag{3.78}$$

Using this definition for $\mathbf{E}_{\mathbf{K}}$ in equation (3.74), the equations of motion for the exciton creation operator, $i\hbar dB^{\dagger}_{\mu,\mathbf{K}}/dt = \left[B^{\dagger}_{\mu,\mathbf{K}}, H\right]$ become

$$i\hbar\frac{dB^{\dagger}_{\mu,\mathbf{K}}}{dt} = \left[B^{\dagger}_{\mu,\mathbf{K}}, H_0^{EX}\right] + \mathcal{S}\sum_{\mathbf{K}'}\frac{1}{\varepsilon}\mathbf{E}_{-\mathbf{K}'}\cdot\left[\mathbf{P}_{\mathbf{K}'}, B^{\dagger}_{\mu,\mathbf{K}}\right] \tag{3.79}$$

where $\mathcal{S}$ symmetrizes the operators in the second term to give $\frac{1}{2}\left(\mathbf{E}_{-\mathbf{K}}\cdot\left[\mathbf{P}_{\mathbf{K}}, B^{\dagger}_{\mu,\mathbf{K}}\right] + \left[\mathbf{P}_{\mathbf{K}}, B^{\dagger}_{\mu,\mathbf{K}}\right]\cdot\mathbf{E}_{-\mathbf{K}}\right)$.[31] Substituting equation (3.75), the commutator $\left[\mathbf{P}_{\mathbf{K}'}, B^{\dagger}_{\mu,\mathbf{K}}\right]$ in equation (3.79) can be written as

$$\left[B^{\dagger}_{\mu,\mathbf{K}}, \mathbf{P}_{\mathbf{K}'}\right] = \frac{1}{V}\left(\sum_{\mu',\mathbf{K}'}\mathbf{M}^{*}_{\mu',\mathbf{K}'}\left[B^{\dagger}_{\mu,\mathbf{K}}, B_{\mu',\mathbf{K}'}\right] + \sum_{\mu',\mathbf{K}',\mu'',\mathbf{K}''}\mathbf{G}_{\mu',\mathbf{K}'-\mathbf{K}'';\mu'',\mathbf{K}''}B^{\dagger}_{\mu',\mathbf{K}'-\mathbf{K}''}\left[B^{\dagger}_{\mu,\mathbf{K}}, B_{\mu'',-\mathbf{K}''}\right]\right). \tag{3.80}$$

where the commutator $\left[B^{\dagger}_{\mu,\mathbf{K}}, B_{\mu'',-\mathbf{K}''}\right]$ takes the form

$$\left[B_{\mu,\mathbf{K}}, B^{\dagger}_{\mu',\mathbf{K}'}\right] = \delta_{\mu,\mu'}\delta_{\mathbf{K},\mathbf{K}'} - 2\sum_{\mu'',\mu'''}X^{\mu,\mu';\mathbf{K}-\mathbf{K}'}_{\mu'',\mu'''}B^{\dagger}_{\mu'',\mathbf{K}'}B_{\mu''',\mathbf{K}}. \tag{3.81}$$

3.5 The correlation functions for $B^{\dagger(22\overline{1})}_{\mu}$

We now need to determine expressions for the interband and intraband correlation functions up to third order in the optical field. By using the product rule from differential calculus, we can determine the time derivatives of the operator products by simply substituting equations (3.79) and (3.81). Once this is done, we need only take the expectation values for each correlation

function.

At this point we will change notations. This is done to maintain consistency with the given literature, as well as to simplify things somewhat. We will first replace the subscript $\mathbf{K}_i$ with the superscript i , and $-\mathbf{K}_i$ with $\bar{i}$; for example $< B^{\dagger}_{\mu,\mathbf{K_2}} >$ becomes $< B^{\dagger}_{\mu} >^{(2)}$, and $\left\langle B_{\mu',-\mathbf{K}_1} \right\rangle$ becomes $< B_{\mu} >^{(\bar{1})}$. The $\mathbf{K}^{th}_i$ Fourier component of the external optical field, $\mathbf{E}^{ext}_{opt,\mathbf{K}_1}$ by $\mathcal{E}_i$ and the external THz field by $\mathbf{E}_{THz}$.[31] Using these changes, we can write the third order correlation function as

$$\begin{aligned} i\hbar\frac{dB^{\dagger}_{\mu}}{dt} + \hbar\omega^0_{\mu}B^{\dagger}_{\mu} &= \mathbf{E}_{opt}\cdot\left[\mathbf{M}^*_{\mu} - 2\sum_{\mu',\mu'',\mu'''}\mathbf{M}^*_{\mu'}X^{\mu',\mu}_{\mu'',\mu'''}B^{\dagger}_{\mu''}B_{\mu'''}\right] \\ &\quad +\mathbf{E}_{THz}\left[\sum_{\mu'}\mathbf{G}_{\mu',\mu}B^{\dagger}_{\mu'} - 2\sum_{\mu',\mu'',\mu''',\mu''''}\mathbf{G}_{\mu'',\mu'}X^{\mu',\mu}_{\mu''',\mu''''}B^{\dagger}_{\mu''}B^{\dagger}_{\mu'''}B_{\mu''''}\right] \\ &\quad -\frac{1}{\varepsilon_0\left(1+\chi_{\parallel}\right)}\frac{1}{V}\sum_{\mu',\mu'',\mu'''}\mathbf{G}_{\mu'',\mu'''}\mathbf{G}_{\mu',\mu}B^{\dagger}_{\mu''}B_{\mu'}B^{\dagger\prime}_{\mu'''} + S_{\mu} \end{aligned} \tag{3.82}$$

where S_{μ} is given by

$$\begin{aligned} S_{\mu} &= \frac{\left(\chi_{\parallel}-1\right)}{2\left(\chi_{\parallel}+1\right)\varepsilon_0 V}\sum_{\mu',\mu''}\mathbf{G}_{\mu'',\mu'}\mathbf{G}_{\mu',\mu}B^{\dagger}_{\mu''} \\ &\quad -\frac{\left(\chi_{\parallel}-1\right)}{\left(\chi_{\parallel}+1\right)\varepsilon_0 V}\sum_{\mu',\mu'',\mu''',\mu'''',\mu'''''}\mathbf{G}_{\mu'',\mu'''}\mathbf{G}_{\mu',\mu}X^{\mu''',\mu'}_{\mu'''',\mu'''''}B^{\dagger}_{\mu''}B^{\dagger}_{\mu''''}B_{\mu'''''} \\ &\quad +\frac{1}{\varepsilon_0 V}\sum_{\mu',\mu'',\mu'''}\mathbf{M}^*_{\mu'}X^{\mu',\mu}_{\mu'',\mu'''}\mathbf{M}_{\mu'''}B^{\dagger}_{\mu''} \\ &\quad -\frac{2}{\varepsilon_0 V}\sum_{\mu',\mu'',\mu''',\mu'''',\mu''''',\mu'''''}\mathbf{M}^*_{\mu'}X^{\mu',\mu}_{\mu'',\mu'''}\mathbf{M}_{\mu''''}X^{\mu''',\mu''''}_{\mu''''',\mu'''''}B^{\dagger}_{\mu''}B^{\dagger}_{\mu''''}B_{\mu'''''} \\ &\quad +\frac{1}{\varepsilon_0 V}\sum_{\mu',\mu'',\mu''',\mu'''',\mu'''''}\{\mathbf{G}_{\mu'''',\mu'''''}\mathbf{G}_{\mu'',\mu'}X^{\mu',\mu}_{\mu''',\mu''''}B^{\dagger}_{\mu''}B^{\dagger}_{\mu'''}B_{\mu'''''} \\ &\quad -\mathbf{G}_{\mu'''''',\mu''}\mathbf{G}_{\mu'',\mu'}X^{\mu',\mu}_{\mu''',\mu''''}B^{\dagger}_{\mu''''}B^{\dagger}_{\mu'''}B_{\mu''''} \\ &\quad -\mathbf{G}_{\mu'''',\mu'''}\mathbf{G}_{\mu'',\mu'}X^{\mu',\mu}_{\mu''',\mu''''}B^{\dagger}_{\mu''''}B^{\dagger}_{\mu''}B_{\mu''''}\} \end{aligned} \tag{3.83}$$

In the limit where V goes to infinity, we can show that the terms in S_{μ} that are linear in $B^{\dagger}_{\mu''}$ go to zero, whereas the last term in the $B^{\dagger}_{\mu''}$ evolution equation is proportional to the density,

and therefore does not. In the simple case of non-interacting pairs with zero inplane motion, we have that

$$X^{\mu,\mu'}_{\mu'',\mu'''} = \frac{1}{N_z}\delta_{\mu,\mu'''}\delta_{\mu',\mu''} \tag{3.84}$$

and that

$$\mathbf{G}_{\mu,\mu'} = -e\mu d\delta_{\mu,\mu'} + eL\left(\delta_{\mu',\mu+1} + \delta_{\mu',\mu-1}\right). \tag{3.85}$$

Using these, we can show that the terms which are linear in $B^{\dagger}_{\mu''}$, as well as the terms containing $\mathbf{M}^{*}_{\mu'}$, both go to zero as $V \to 0$, but the remaining terms are proportional to the density. This leaves us with the simplified version for S_μ in the limit of V goes to zero:

$$\begin{aligned} S_\mu &= -\frac{\left(\chi_\parallel - 1\right)}{\left(\chi_\parallel + 1\right)\varepsilon_0 V}\sum_{\mu',\mu'',\mu''',\mu'''',\mu'''''} \mathbf{G}_{\mu'',\mu'''}\mathbf{G}_{\mu',\mu}X^{\mu''',\mu'}_{\mu'''',\mu'''''}B^{\dagger}_{\mu''}B^{\dagger}_{\mu''''}B_{\mu''''} \\ &\quad + \frac{1}{\varepsilon_0 V}\sum_{\mu',\mu'',\mu''',\mu'''',\mu'''''} \{\mathbf{G}_{\mu'''',\mu'''''}\mathbf{G}_{\mu'',\mu'}X^{\mu',\mu}_{\mu''',\mu''''}B^{\dagger}_{\mu''}B^{\dagger}_{\mu'''}B_{\mu'''''} \\ &\quad - \mathbf{G}_{\mu''''',\mu''}\mathbf{G}_{\mu'',\mu'}X^{\mu',\mu}_{\mu''',\mu''''}B^{\dagger}_{\mu'''''}B^{\dagger}_{\mu'''}B_{\mu''''} \\ &\quad - \mathbf{G}_{\mu''''',\mu'''}\mathbf{G}_{\mu'',\mu'}X^{\mu',\mu}_{\mu''',\mu''''}B^{\dagger}_{\mu'''''}B^{\dagger}_{\mu''}B_{\mu''''}\} \end{aligned} \tag{3.86}$$

We can now see that S_μ deals entirely with phase-space corrections$\left(X^{\mu,\mu'}_{\mu'',\mu'''}\right)$.

Now that we have an equation for the correlation functions, we can begin to determine the form of the lower order equations. We will begin with the first order ones. In order to find these, we take the third order equation, (3.82), and drop all terms which are higher than first order in B. This gives us the following equations, one for each of the two exciting optical fields

$$i\hbar\frac{d\left\langle B^{\dagger(2)}_{\mu}\right\rangle}{dt} + \hbar\omega^{0}_{\mu}\left\langle B^{\dagger}_{\mu}\right\rangle^{(2)} = \mathcal{E}^{*}_{2}(t)e^{i\boldsymbol{\omega}_c t}\cdot\mathbf{M}^{*}_{\mu} + \mathbf{E}_{\perp THz}\cdot\sum_{\mu'}\mathbf{G}_{\mu',\mu}\left\langle B^{\dagger}_{\mu'}\right\rangle^{(2)} \tag{3.87}$$

$$i\hbar\frac{d\left\langle B^{(1)}_{\mu}\right\rangle}{dt} - \hbar\omega^{0}_{\mu}\left\langle B_{\mu}\right\rangle^{(\bar{1})} = \mathcal{E}_{1}(t)e^{-i\boldsymbol{\omega}_c t}\cdot\mathbf{M}_{\mu} - \mathbf{E}_{\perp THz}\cdot\sum_{\mu'}\mathbf{G}^{*}_{\mu',\mu}\left\langle B_{\mu'}\right\rangle^{(\bar{1})} \tag{3.88}$$

In the section on DFWM experiments, we showed that the signal we are interested in has a

dependance on the direction $2\mathbf{K}_2 - \mathbf{K}_1$. In order to evaluate the intensity of this signal, we will need the equation for $\left\langle B_\mu^\dagger \right\rangle^{(22\overline{1})}$. This is given by the following:

$$\begin{aligned} i\hbar \frac{d\left\langle B_\mu^\dagger \right\rangle^{(22\overline{1})}}{dt} &= -\hbar\omega_\mu^0 \left\langle B_\mu^\dagger \right\rangle^{(22\overline{1})} - 2\mathcal{E}_2^*(t) e^{i\boldsymbol{\omega}_c t} \cdot \left[\sum_{\mu',\mu'',\mu'''} \mathbf{M}_{\mu'}^* X_{\mu'',\mu'''}^{\mu',\mu} \left\langle B_{\mu''}^\dagger B_{\mu'''} \right\rangle^{(2\overline{1})} \right] \\ &\quad + \mathbf{E}_{\perp THz} \sum_{\mu'} \mathbf{G}_{\mu',\mu} \left\langle B_{\mu'}^\dagger \right\rangle^{(22\overline{1})} \\ &\quad - 2\mathbf{E}_{\perp THz} \sum_{\mu',\mu'',\mu''',\mu''''} \mathbf{G}_{\mu'',\mu'} X_{\mu''',\mu''''}^{\mu',\mu} \left\langle B_{\mu''}^\dagger B_{\mu'''}^\dagger B_{\mu''''} \right\rangle^{(22\overline{1})} \\ &\quad - \frac{1}{\varepsilon_0 \left(1 + \chi_\parallel\right)} \frac{1}{V} \sum_{\mu',\mu'',\mu'''} \mathbf{G}_{\mu'',\mu'''} \mathbf{G}_{\mu',\mu} \left\langle B_{\mu''}^\dagger B_{\mu'}^\dagger B_{\mu'''}' \right\rangle^{(22\overline{1})} + \langle S_\mu \rangle \end{aligned} \tag{3.89}$$

Looking at this equation, we can see that there are two quantities which we do not have equations for. These are $\left\langle B_\mu^\dagger B_{\mu'} \right\rangle^{(2\overline{1})}$ and $\left\langle B_\mu^\dagger B_{\mu'}^\dagger B_{\mu''} \right\rangle^{(22\overline{1})}$. By using the product rule, as mentioned above, we can create equations for these by combining the first order equations (3.87) and (3.88).

$$\begin{aligned} i\hbar \frac{dB_\mu^\dagger B_{\mu'}}{dt} &= i\hbar \frac{dB_\mu^\dagger}{dt} B_{\mu'} + i\hbar B_\mu^\dagger \frac{dB_{\mu'}}{dt} & (3.90) \\ &= \left(\hbar\omega_{\mu'}^0 - \hbar\omega_\mu^0\right) B_\mu^\dagger B_{\mu'} + \mathbf{E}_{\perp opt} \cdot \left(\mathbf{M}_\mu^* B_{\mu'} - \mathbf{M}_{\mu'} B_\mu^\dagger \right) \\ &\quad + \mathbf{E}_{\perp THz} \cdot \sum_{\mu''} \left(\mathbf{G}_{\mu'',\mu} B_{\mu''}^\dagger B_{\mu'} - \mathbf{G}_{\mu'',\mu'}^* B_\mu^\dagger B_{\mu''} \right) & (3.91) \end{aligned}$$

Taking expectation values gives us

$$\begin{aligned} i\hbar \frac{d\left\langle B_\mu^\dagger B_{\mu'} \right\rangle^{(2\overline{1})}}{dt} &= \left(\hbar\omega_{\mu'}^0 - \hbar\omega_\mu^0\right) \left\langle B_\mu^\dagger B_{\mu'} \right\rangle^{(2\overline{1})} + \mathcal{E}_2^*(t) e^{i\boldsymbol{\omega}_c t} \mathbf{M}_\mu^* \left\langle B_{\mu'} \right\rangle^{(\overline{1})} \\ &\quad - \mathcal{E}_1(t) e^{-i\boldsymbol{\omega}_c t} \mathbf{M}_{\mu'} \left\langle B_\mu^\dagger \right\rangle^{(2)} \\ &\quad + \mathbf{E}_{\perp THz} \cdot \sum_{\mu''} \left(\mathbf{G}_{\mu'',\mu} \left\langle B_{\mu''}^\dagger B_{\mu'} \right\rangle^{(2\overline{1})} - \mathbf{G}_{\mu'',\mu'}^* \left\langle B_\mu^\dagger B_{\mu''} \right\rangle^{(2\overline{1})} \right) \end{aligned} \tag{3.92}$$

In order to get the equations for $\left\langle B_{\mu}^{\dagger}B_{\mu'}^{\dagger}B_{\mu''}\right\rangle^{(22\overline{1})}$, we use a similar process.

$$
\begin{aligned}
i\hbar\frac{dB_{\mu}^{\dagger}B_{\mu'}^{\dagger}B_{\mu''}}{dt} &= i\hbar B_{\mu}^{\dagger}\frac{dB_{\mu'}^{\dagger}B_{\mu''}}{dt}+i\hbar\frac{dB_{\mu}^{\dagger}}{dt}B_{\mu'}^{\dagger}B_{\mu''} && (3.93)\\
&= \left(\hbar\omega_{\mu''}^{0}-\hbar\omega_{\mu'}^{0}\right)B_{\mu}^{\dagger}B_{\mu'}^{\dagger}B_{\mu''}+\mathbf{E}_{\perp opt}\cdot\left(\mathbf{M}_{\mu'}^{*}B_{\mu}^{\dagger}B_{\mu''}-\mathbf{M}_{\mu''}B_{\mu}^{\dagger}B_{\mu'}^{\dagger}\right)\\
&\quad+\mathbf{E}_{\perp THz}\cdot\sum_{\mu'''}\left(\mathbf{G}_{\mu''',\mu'}B_{\mu}^{\dagger}B_{\mu'''}^{\dagger}B_{\mu''}-\mathbf{G}_{\mu''',\mu''}^{*}B_{\mu}^{\dagger}B_{\mu'}^{\dagger}B_{\mu'''}\right)\\
&\quad-\hbar\omega_{\mu}^{0}B_{\mu}^{\dagger}B_{\mu'}^{\dagger}B_{\mu''}+\mathbf{E}_{\perp opt}\cdot\mathbf{M}_{\mu}^{*}B_{\mu'}^{\dagger}B_{\mu''}\\
&\quad+\mathbf{E}_{\perp THz}\cdot\sum_{\mu'''}\mathbf{G}_{\mu''',\mu}B_{\mu'''}^{\dagger}B_{\mu'}^{\dagger}B_{\mu''} && (3.94)
\end{aligned}
$$

After taking expectation values as before, we obtain:

$$
\begin{aligned}
i\hbar\frac{d\left\langle B_{\mu}^{\dagger}B_{\mu'}^{\dagger}B_{\mu''}\right\rangle^{(22\overline{1})}}{dt} &= i\hbar B_{\mu}^{\dagger}\frac{dB_{\mu'}^{\dagger}B_{\mu''}}{dt}+i\hbar\frac{dB_{\mu}^{\dagger}}{dt}B_{\mu'}^{\dagger}B_{\mu''} && (3.95)\\
&= \left(\hbar\omega_{\mu''}^{0}-\hbar\omega_{\mu'}^{0}-\hbar\omega_{\mu}^{0}\right)\left\langle B_{\mu}^{\dagger}B_{\mu'}^{\dagger}B_{\mu''}\right\rangle^{(22\overline{1})}\\
&\quad+\mathcal{E}_{2}^{*}(t)e^{i\boldsymbol{\omega}_{c}t}\mathbf{M}_{\mu'}^{*}\left\langle B_{\mu}^{\dagger}B_{\mu''}\right\rangle^{(2\overline{1})}-\mathcal{E}_{1}(t)e^{-i\boldsymbol{\omega}_{c}t}\mathbf{M}_{\mu''}\left\langle B_{\mu}^{\dagger}B_{\mu'}^{\dagger}\right\rangle^{(22)}\\
&\quad+\mathcal{E}_{2}^{*}(t)e^{i\boldsymbol{\omega}_{c}t}\mathbf{M}_{\mu}^{*}\left\langle B_{\mu'}^{\dagger}B_{\mu''}\right\rangle^{(2\overline{1})}\\
&\quad+\mathbf{E}_{\perp THz}\cdot\sum_{\mu'''}(\mathbf{G}_{\mu''',\mu'}\left\langle B_{\mu}^{\dagger}B_{\mu'''}^{\dagger}B_{\mu''}\right\rangle^{(22\overline{1})}\\
&\quad-\mathbf{G}_{\mu''',\mu''}^{*}\left\langle B_{\mu}^{\dagger}B_{\mu'}^{\dagger}B_{\mu'''}\right\rangle^{(22\overline{1})}+\mathbf{G}_{\mu''',\mu}\left\langle B_{\mu'''}^{\dagger}B_{\mu'}^{\dagger}B_{\mu''}\right\rangle^{(22\overline{1})}) && (3.96)
\end{aligned}
$$

Looking at this last equation, you can see that a new term has appeared, $\left\langle B_{\mu}^{\dagger}B_{\mu'}^{\dagger}\right\rangle^{(22)}$. We will need to find the equations of motion for this term as well.

$$
\begin{aligned}
i\hbar\frac{dB_{\mu}^{\dagger}B_{\mu'}^{\dagger}}{dt} &= i\hbar\frac{dB_{\mu}^{\dagger}}{dt}B_{\mu'}^{\dagger}+i\hbar B_{\mu}^{\dagger}\frac{dB_{\mu'}^{\dagger}}{dt} && (3.97)\\
&= -\left(\hbar\omega_{\mu'}^{0}+\hbar\omega_{\mu}^{0}\right)B_{\mu}^{\dagger}B_{\mu'}^{\dagger}+\mathbf{E}_{\perp opt}\cdot\left(\mathbf{M}_{\mu}^{*}B_{\mu'}^{\dagger}+\mathbf{M}_{\mu'}B_{\mu}^{\dagger}\right)\\
&\quad+\mathbf{E}_{\perp THz}\cdot\sum_{\mu''}\left(\mathbf{G}_{\mu'',\mu}B_{\mu''}^{\dagger}B_{\mu'}^{\dagger}+\mathbf{G}_{\mu'',\mu'}^{*}B_{\mu}^{\dagger}B_{\mu''}^{\dagger}\right) && (3.98)
\end{aligned}
$$

We obtain, after taking expectation values:

$$\begin{aligned} i\hbar\frac{d\left\langle B_{\mu}^{\dagger}B_{\mu'}^{\dagger}\right\rangle^{(22)}}{dt} &= -\left(\hbar\omega_{\mu'}^{0}+\hbar\omega_{\mu}^{0}\right)\left\langle B_{\mu}^{\dagger}B_{\mu'}^{\dagger}\right\rangle^{(22)} \\ &+\mathcal{E}_{2}^{*}(t)e^{i\boldsymbol{\omega}_{c}t}\left(\mathbf{M}_{\mu}^{*}\left\langle B_{\mu'}^{\dagger}\right\rangle^{(2)}+\mathbf{M}_{\mu'}\left\langle B_{\mu}^{\dagger}\right\rangle^{(2)}\right) \\ &+\mathbf{E}_{\perp THz}\cdot\sum_{\mu''}\left(\mathbf{G}_{\mu'',\mu}\left\langle B_{\mu''}^{\dagger}B_{\mu'}^{\dagger}\right\rangle^{(22)}+\mathbf{G}_{\mu'',\mu'}^{*}\left\langle B_{\mu}^{\dagger}B_{\mu''}^{\dagger}\right\rangle^{(22)}\right). \end{aligned} \tag{3.99}$$

3.5.1 Including Phenomenological Dephasing Decay

If we assume that the full Hamiltonian is actually $H_{full} = H + H_{other}$, where H_{other} includes effects such as carrier-carrier scattering, phonon-electron interactions, as well as impurities and defects in the crystal, and H is the Hamiltonian we have been using above to create the equations of motion in the coherent limit. In order to include this decay, we can simply assume that the following commutation relationships apply to H_{other}:

$$\left\langle\left[B_{\mu}^{\dagger},H_{other}\right]\right\rangle = \frac{\left\langle B_{\mu}^{\dagger}\right\rangle}{T_{\mu}}, \tag{3.100}$$

$$\left\langle\left[B_{\mu}^{\dagger}B_{\mu'},H_{other}\right]\right\rangle = \frac{\left\langle B_{\mu}^{\dagger}B_{\mu'}\right\rangle}{T_{\mu\mu'}}, \tag{3.101}$$

$$\left\langle\left[B_{\mu}^{\dagger}B_{\mu'}^{\dagger},H_{other}\right]\right\rangle = \frac{\left\langle B_{\mu}^{\dagger}B_{\mu'}^{\dagger}\right\rangle}{T'_{\mu\mu'}}, \tag{3.102}$$

$$\left\langle\left[B_{\mu}^{\dagger}B_{\mu'}^{\dagger}B_{\mu''},H_{other}\right]\right\rangle = \frac{\left\langle B_{\mu}^{\dagger}B_{\mu'}^{\dagger}B_{\mu''}\right\rangle}{T_{\mu\mu'\mu''}}. \tag{3.103}$$

Applying these, we obtain the final equations of motion:

$$i\hbar\frac{d\left\langle B_{\mu}^{\dagger(2)}\right\rangle}{dt}+\left(\hbar\omega_{\mu}^{0}+\frac{i\hbar}{T_{\mu}}\right)\left\langle B_{\mu}^{\dagger}\right\rangle^{(2)} = \mathcal{E}_{2}^{*}(t)e^{i\boldsymbol{\omega}_{c}t}\cdot\mathbf{M}_{\mu}^{*} + \mathbf{E}_{\perp THz}\cdot\sum_{\mu'}\mathbf{G}_{\mu',\mu}\left\langle B_{\mu'}^{\dagger}\right\rangle^{(2)} \quad (3.104)$$

$$i\hbar\frac{d\left\langle B_{\mu}\right\rangle^{(\bar{1})}}{dt}+\left(-\hbar\omega_{\mu}^{0}+\frac{i\hbar}{T_{\mu}}\right)\left\langle B_{\mu}\right\rangle^{(\bar{1})} = \mathcal{E}_{1}(t)e^{-i\boldsymbol{\omega}_{c}t}\cdot\mathbf{M}_{\mu} - \mathbf{E}_{\perp THz}\cdot\sum_{\mu'}\mathbf{G}_{\mu',\mu}^{*}\left\langle B_{\mu'}\right\rangle^{(\bar{1})} \quad (3.105)$$

$$\begin{aligned} i\hbar\frac{d\left\langle B_{\mu}^{\dagger}B_{\mu'}\right\rangle^{(2\bar{1})}}{dt} &= \left(\hbar\omega_{\mu'}^{0}-\hbar\omega_{\mu}^{0}-\frac{i\hbar}{T_{\mu\mu'}}\right)\left\langle B_{\mu}^{\dagger}B_{\mu'}\right\rangle^{(2\bar{1})} \\ &+\mathcal{E}_{2}^{*}(t)e^{i\boldsymbol{\omega}_{c}t}\mathbf{M}_{\mu}^{*}\left\langle B_{\mu'}\right\rangle^{(\bar{1})}-\mathcal{E}_{1}^{*}(t)e^{-i\boldsymbol{\omega}_{c}t}\mathbf{M}_{\mu'}\left\langle B_{\mu}^{\dagger}\right\rangle^{(2)} \\ &+\mathbf{E}_{\perp THz}\cdot\sum_{\mu''}\left[\mathbf{G}_{\mu'',\mu}\left\langle B_{\mu''}^{\dagger}B_{\mu'}\right\rangle^{(2\bar{1})}-\mathbf{G}_{\mu'',\mu'}^{*}\left\langle B_{\mu}^{\dagger}B_{\mu''}\right\rangle^{(2\bar{1})}\right] \end{aligned} \quad (3.106)$$

$$\begin{aligned} i\hbar\frac{d\left\langle B_{\mu}^{\dagger}B_{\mu'}^{\dagger}\right\rangle^{(22)}}{dt} &= -\left(\hbar\omega_{\mu'}^{0}+\hbar\omega_{\mu}^{0}+\frac{i\hbar}{T'_{\mu\mu'}}\right)\left\langle B_{\mu}^{\dagger}B_{\mu'}^{\dagger}\right\rangle^{(22)} \\ &+\mathcal{E}_{2}^{*}(t)e^{i\boldsymbol{\omega}_{c}t}\left(\mathbf{M}_{\mu}^{*}\left\langle B_{\mu'}^{\dagger}\right\rangle^{(2)}+\mathbf{M}_{\mu'}\left\langle B_{\mu}^{\dagger}\right\rangle^{(2)}\right) \\ &+\mathbf{E}_{\perp THz}\cdot\sum_{\mu''}\left(\mathbf{G}_{\mu'',\mu}\left\langle B_{\mu''}^{\dagger}B_{\mu'}^{\dagger}\right\rangle^{(22)}+\mathbf{G}_{\mu'',\mu'}^{*}\left\langle B_{\mu}^{\dagger}B_{\mu''}^{\dagger}\right\rangle^{(22)}\right) \end{aligned} \quad (3.107)$$

$$
\begin{aligned}
i\hbar\frac{d\left\langle B_{\mu}^{\dagger}B_{\mu'}^{\dagger}B_{\mu''}\right\rangle^{(22\overline{1})}}{dt} &= \left(\hbar\omega_{\mu''}^{0}-\hbar\omega_{\mu'}^{0}-\hbar\omega_{\mu}^{0}-\frac{i\hbar}{T'_{\mu\mu'\mu''}}\right)\left\langle B_{\mu}^{\dagger}B_{\mu'}^{\dagger}B_{\mu''}\right\rangle^{(22\overline{1})} \\
&+\mathcal{E}_{2}^{*}(t)e^{i\boldsymbol{\omega}_{c}t}\mathbf{M}_{\mu'}^{*}\left\langle B_{\mu}^{\dagger}B_{\mu''}\right\rangle^{(2\overline{1})} \\
&-\mathcal{E}_{1}^{*}(t)e^{-i\boldsymbol{\omega}_{c}t}\mathbf{M}_{\mu''}\left\langle B_{\mu}^{\dagger}B_{\mu'}^{\dagger}\right\rangle^{(22)}+\mathcal{E}_{2}^{*}(t)e^{i\boldsymbol{\omega}_{c}t}\mathbf{M}_{\mu}^{*}\left\langle B_{\mu'}^{\dagger}B_{\mu''}\right\rangle^{(2\overline{1})} \\
&+\mathbf{E}_{\perp THz}\cdot\sum_{\mu'''}(\mathbf{G}_{\mu''',\mu'}\left\langle B_{\mu}^{\dagger}B_{\mu'''}^{\dagger}B_{\mu''}\right\rangle^{(22\overline{1})} \\
&-\mathbf{G}_{\mu''',\mu''}^{*}\left\langle B_{\mu}^{\dagger}B_{\mu'}^{\dagger}B_{\mu'''}\right\rangle^{(22\overline{1})}+\mathbf{G}_{\mu''',\mu}\left\langle B_{\mu'''}^{\dagger}B_{\mu'}^{\dagger}B_{\mu''}\right\rangle^{(22\overline{1})}) \qquad (3.108)
\end{aligned}
$$

$$
\begin{aligned}
i\hbar\frac{d\left\langle B_{\mu}^{\dagger}\right\rangle^{(22\overline{1})}}{dt} &= -\left(\hbar\omega_{\mu}^{0}+\frac{i\hbar}{T_{\mu}}\right)\left\langle B_{\mu}^{\dagger}\right\rangle^{(22\overline{1})}-2\mathcal{E}_{2}^{*}(t)e^{i\boldsymbol{\omega}_{c}t}\cdot\left[\sum_{\mu',\mu'',\mu'''}\mathbf{M}_{\mu'}^{*}X_{\mu'',\mu'''}^{\mu',\mu}\left\langle B_{\mu''}^{\dagger}B_{\mu'''}\right\rangle^{(2\overline{1})}\right] \\
&+\mathbf{E}_{\perp THz}\sum_{\mu'}\mathbf{G}_{\mu',\mu}\left\langle B_{\mu'}^{\dagger}\right\rangle^{(22\overline{1})} \\
&-2\mathbf{E}_{\perp THz}\sum_{\mu',\mu'',\mu''',\mu''''}\mathbf{G}_{\mu'',\mu'}X_{\mu''',\mu''''}^{\mu',\mu}\left\langle B_{\mu''}^{\dagger}B_{\mu'''}^{\dagger}B_{\mu''''}\right\rangle^{(22\overline{1})} \\
&-\frac{1}{\varepsilon_{0}\left(1+\chi_{\parallel}\right)}\frac{1}{V}\sum_{\mu',\mu'',\mu'''}\mathbf{G}_{\mu'',\mu'''}\mathbf{G}_{\mu',\mu}\left\langle B_{\mu''}^{\dagger}B_{\mu'}^{\dagger}B_{\mu'''}^{\prime}\right\rangle^{(22\overline{1})}+\langle S_{\mu}\rangle \qquad (3.109)
\end{aligned}
$$

These are the sets of equations we must solve simultaneously in order to obtain the third order polarization in the $2\mathbf{K}_2-\mathbf{K}_1$ direction for a DFWM experiment, This polarization is given by

$$
\langle\mathbf{P}_{iner}\rangle^{(22\overline{1})}=\frac{2}{V}\,\mathrm{Re}\left\{\sum_{\mu}\mathbf{M}_{\mu}\left\langle B_{\mu}^{\dagger}\right\rangle^{(22\overline{1})}\right\} \qquad (3.110)
$$

In order to solve these equations numerically, it is necessary to put them into a dimensionless form, as well as factor out the time dependance. This will require redefining several of the parameters involved in the DFWM equations.

One of the parameters which we wish to remove is volume. To do so, we make the following definitions:

$$
X_{\mu'',\mu'''}^{\mu,\mu'}=\frac{da_{0}^{2}}{V}Y_{\mu'',\mu'''}^{\mu,\mu'} \qquad (3.111)
$$

We will also define

$$\mathbf{M}_{\mu} = \mathbf{M}_0 S_{\mu} \sqrt{\frac{V}{d}} \tag{3.112}$$

By these definitions, $\mathbf{M}_0$ is the bulk dipole matrix element between the conduction and valence bands, with units of charge·length, and

$$\begin{aligned} S_{\mu} &= \frac{1}{\sqrt{N_z}} \int dz \Psi^{\mu}\left(r=0,z,z\right) && (3.113) \\ &= \frac{\widetilde{S}_{\mu}}{a_0}, && (3.114) \end{aligned}$$

with the units of one over length, and

$$\Psi^{\mu}\left(r,z,z\right) = \frac{1}{\sqrt{N_z}} \sum_{n,\beta} D^{\mu}_{\beta,l} f_h\left(z_h - nd\right) f_e\left(z_e - \left(n+l\right)d\right) \phi^{\beta}_{l}\left(r\right) \tag{3.115}$$

This last equation is the wavefunction without the inplane center of mass motion included, which would give a factor of $1/\sqrt{A}$. The purpose of these definitions is to remove the problematic factors of V which appear in the equations of motion. Once these are removed, we can solve these systems on the computer.

We will also introduce a dimensionless intraband dipole matrix element:

$$\widetilde{G}_{\mu,\nu} = -\frac{G_{\mu,\nu}}{ed} \tag{3.116}$$

as well as

$$B_{\mu}\left(\tau/\omega_B\right) = \frac{e}{\mathbf{M}^*_0} K_{\mu}\left(\tau\right) e^{-i\omega^0_{\mu}\tau}, \text{ where } \tau = \omega_B t. \tag{3.117}$$

Finally, we define

$$\Gamma_{\mu} = \omega_B T_{\mu} \tag{3.118}$$

with similar definitions for the rest of the dephasing times, and

$$\widetilde{\omega}_\mu = \frac{\omega_\mu}{\omega_B}. \tag{3.119}$$

Using all of these in our equations of motion gives us the following:

$$\begin{aligned}\frac{d\left\langle K_\mu\right\rangle^{(\bar{1})}}{d\tau} + \frac{1}{\Gamma_\mu}\left\langle K_\mu\right\rangle^{(\bar{1})} &= i\mathcal{E}_1(\tau/\omega_B)e^{-i\left(\widetilde{\omega}_c-\widetilde{\omega}^0_\mu\right)\tau}\cdot\widetilde{S}_\mu\frac{|\mathbf{M}_o|^2}{a_o\hbar\omega_B} \\ &\quad -i\frac{d\mathbf{E}_{THz}}{\hbar\omega_B}\cdot\sum_{\mu'}\widetilde{\mathbf{G}}^*_{\mu',\mu}\left\langle K_{\mu'}\right\rangle^{(\bar{1})}e^{-i\left(\widetilde{\omega}^0_{\mu'}-\widetilde{\omega}^0_\mu\right)\tau}, \end{aligned}\tag{3.120}$$

$$\begin{aligned}\frac{d\left\langle K^\dagger_\mu\right\rangle^{(2)}}{d\tau} + \frac{1}{\Gamma_\mu}\left\langle K^\dagger_\mu\right\rangle^{(2)} &= -i\mathcal{E}^*_2(\tau/\omega_B)e^{i\left(\widetilde{\omega}_c-\widetilde{\omega}^0_\mu\right)\tau}\cdot\widetilde{S}_\mu\frac{|\mathbf{M}_o|^2}{a_o\hbar\omega_B} \\ &\quad +i\frac{d\mathbf{E}_{THz}}{\hbar\omega_B}\cdot\sum_{\mu'}\widetilde{\mathbf{G}}_{\mu',\mu}\left\langle K^\dagger_{\mu'}\right\rangle^{(2)}e^{i\left(\widetilde{\omega}^0_{\mu'}-\widetilde{\omega}^0_\mu\right)\tau}, \end{aligned}\tag{3.121}$$

$$\begin{aligned}\frac{d\left\langle K^\dagger_\mu K_\nu\right\rangle^{(2\bar{1})}}{d\tau} &= -\frac{1}{\Gamma_{\mu\nu}}\left\langle K^\dagger_\mu K_\nu\right\rangle^{(2\bar{1})} + -i\mathcal{E}^*_2(\tau/\omega_B)e^{i\left(\widetilde{\omega}_c-\widetilde{\omega}^0_\mu\right)\tau}\cdot\widetilde{S}^*_\mu\frac{|\mathbf{M}_o|^2}{a_o e\hbar\omega_B}\left\langle K_\nu\right\rangle^{(\bar{1})} \\ &\quad +i\mathcal{E}_1(\tau/\omega_B)e^{i\left(-\widetilde{\omega}_c+\widetilde{\omega}^0_\nu\right)\tau}\cdot\widetilde{S}_\nu\frac{|\mathbf{M}_o|^2}{a_o e\hbar\omega_B}\left\langle K^\dagger_\mu\right\rangle^{(2)} \\ &\quad +i\frac{ed\mathbf{E}_{\perp THz}}{\hbar\omega_B}\cdot\sum_{\mu'}(\widetilde{\mathbf{G}}_{\mu',\mu}\left\langle K^\dagger_{\mu'}K_\nu\right\rangle^{(2\bar{1})}e^{i\left(\widetilde{\omega}^0_{\mu'}-\widetilde{\omega}^0_\mu\right)\tau} \\ &\quad -\widetilde{\mathbf{G}}^*_{\mu',\nu}\left\langle K^\dagger_\mu K_{\mu'}\right\rangle^{(2\bar{1})}e^{-i\left(\widetilde{\omega}^0_{\mu'}-\widetilde{\omega}^0_\nu\right)\tau}), \end{aligned}\tag{3.122}$$

$$\begin{aligned}\frac{d\left\langle K^\dagger_\mu K^\dagger_\nu\right\rangle^{(22)}}{d\tau} &= -\frac{1}{\Gamma'_{\mu\mu'}}\left\langle K^\dagger_\mu K^\dagger_\nu\right\rangle^{(22)} + -i\mathcal{E}^*_2(\tau/\omega_B)\cdot\frac{|\mathbf{M}_o|^2}{a_o e\hbar\omega_B}e^{i\left(\widetilde{\omega}_c-\widetilde{\omega}^0_\mu\right)\tau}\widetilde{S}^*_\mu\left\langle K^\dagger_\nu\right\rangle^{(2)} \\ &\quad + - i\mathcal{E}^*_2(\tau/\omega_B)\cdot\frac{|\mathbf{M}_o|^2}{a_o e\hbar\omega_B}e^{i\left(\widetilde{\omega}_c-\widetilde{\omega}^0_\nu\right)\tau}\widetilde{S}^*_\nu\left\langle K^\dagger_\mu\right\rangle^{(2)} \\ &\quad +i\frac{ed\mathbf{E}_{\perp THz}}{\hbar\omega_B}\cdot\sum_{\mu'}(\widetilde{\mathbf{G}}_{\mu',\mu}\left\langle K^\dagger_{\mu'}K^\dagger_\nu\right\rangle^{(22)}e^{i\left(\widetilde{\omega}^0_{\mu'}-\widetilde{\omega}^0_\mu\right)\tau} \\ &\quad +\widetilde{\mathbf{G}}_{\mu',\nu}\left\langle K^\dagger_\mu K^\dagger_{\mu'}\right\rangle^{(22)}e^{i\left(\widetilde{\omega}^0_{\mu'}-\widetilde{\omega}^0_\nu\right)\tau}), \end{aligned}\tag{3.123}$$

$$
\begin{aligned}
\frac{d\left\langle K_{\mu}^{\dagger}K_{\mu'}^{\dagger}K_{\mu''}\right\rangle^{(22\overline{1})}}{d\tau} &= -\frac{1}{\Gamma_{\mu\mu'\mu''}}\left\langle K_{\mu}^{\dagger}K_{\mu'}^{\dagger}K_{\mu''}\right\rangle^{(22\overline{1})} \\
&-i\mathcal{E}_2^*(\tau/\omega_B)e^{i\left(\widetilde{\omega}_c-\widetilde{\omega}_{\mu'}^0\right)\tau}\cdot\frac{|\mathbf{M}_o|^2}{a_o e\hbar\omega_B}\widetilde{S}_{\mu'}^*\left\langle K_{\mu}^{\dagger}K_{\mu''}\right\rangle^{(2\overline{1})} \\
&+i\mathcal{E}_1(\tau/\omega_B)e^{-i\left(\widetilde{\omega}_c-\widetilde{\omega}_{\mu''}^0\right)\tau}\frac{|\mathbf{M}_o|^2}{a_o e\hbar\omega_B}\widetilde{S}_{\mu''}\left\langle K_{\mu}^{\dagger}K_{\mu'}^{\dagger}\right\rangle^{(22)} \\
&-i\mathcal{E}_2^*(\tau/\omega_B)e^{i(\widetilde{\omega}_c-\widetilde{\omega}_{\mu}^0)\tau}\cdot\frac{|\mathbf{M}_o|^2}{a_o e\hbar\omega_B}\widetilde{S}_{\mu'}^*\left\langle K_{\mu'}^{\dagger}K_{\mu''}\right\rangle^{(2\overline{1})} \\
&+i\frac{ed\mathbf{E}_{\perp THz}}{\hbar\omega_B}\cdot\sum_{\mu'''}(\widetilde{\mathbf{G}}_{\mu''',\mu'}\left\langle K_{\mu}^{\dagger}K_{\mu'''}^{\dagger}K_{\mu''}\right\rangle^{(22\overline{1})}e^{i\left(\widetilde{\omega}_{\mu'''}^0-\widetilde{\omega}_{\mu'}^0\right)\tau} \\
&-\widetilde{\mathbf{G}}_{\mu''',\mu''}^*\left\langle K_{\mu}^{\dagger}K_{\mu'}^{\dagger}K_{\mu'''}\right\rangle^{(22\overline{1})}e^{-i\left(\widetilde{\omega}_{\mu'''}^0-\widetilde{\omega}_{\mu''}^0\right)\tau} \\
&+\sum_{\mu'''}\widetilde{\mathbf{G}}_{\mu''',\mu}\left\langle K_{\mu'''}^{\dagger}K_{\mu'}^{\dagger}K_{\mu''}\right\rangle^{(22\overline{1})}e^{i\left(\widetilde{\omega}_{\mu'''}^0-\widetilde{\omega}_{\mu}^0\right)\tau}), \qquad (3.124)
\end{aligned}
$$

$$
\begin{aligned}
\frac{d\left\langle K_{\mu}^{\dagger}\right\rangle^{(22\overline{1})}}{d\tau} &= +i\frac{2ea_o\mathcal{E}_2^*(\tau/\omega_B)}{\hbar\omega_B}\cdot\sum_{\mu',\mu'',\mu'''}\widetilde{S}_{\mu'}^*Y_{\mu'',\mu'''}^{\mu',\mu}\left\langle K_{\mu''}^{\dagger}K_{\mu'''}\right\rangle^{(2\overline{1})}e^{i\left(\widetilde{\omega}_c-\widetilde{\omega}_{\mu}^0+\widetilde{\omega}_{\mu''}^0-\widetilde{\omega}_{\mu'''}^0\right)\tau} \\
&+i\frac{ed\mathbf{E}_{\perp THz}}{\hbar\omega_B}\cdot[\sum_{\mu'}\widetilde{\mathbf{G}}_{\mu',\mu}\left\langle K_{\mu'}^{\dagger}\right\rangle^{(22\overline{1})}e^{i\left(\widetilde{\omega}_{\mu'}^0-\widetilde{\omega}_{\mu}^0\right)\tau} \\
&-2\frac{e^2a_o^2}{|\mathbf{M}_o|^2}\sum_{\mu'\mu''\mu'''\mu''''}\widetilde{\mathbf{G}}_{\mu'',\mu'}Y_{\mu''',\mu''''}^{\mu',\mu} \\
&\cdot\left\langle K_{\mu''}^{\dagger}K_{\mu'''}^{\dagger}K_{\mu''''}\right\rangle^{(22\overline{1})}e^{i\left(\widetilde{\omega}_{\mu''}^0+\widetilde{\omega}_{\mu'''}^0-\widetilde{\omega}_{\mu}^0-\widetilde{\omega}_{\mu''''}^0\right)\tau}] \\
&+\frac{i}{\varepsilon_0\left(1+\chi_{\parallel}\right)}\frac{e^4d}{|\mathbf{M}_o|^2\hbar\omega_B}\sum_{\mu',\mu'',\mu'''}\widetilde{\mathbf{G}}_{\mu'',\mu'''} \\
&\cdot\widetilde{\mathbf{G}}_{\mu',\mu}\left\langle K_{\mu''}^{\dagger}K_{\mu'}^{\dagger}K_{\mu'''}\right\rangle^{(22\overline{1})}e^{i\left(\widetilde{\omega}_{\mu''}^0+\widetilde{\omega}_{\mu'}^0-\widetilde{\omega}_{\mu}^0-\widetilde{\omega}_{\mu'''}^0\right)\tau} \\
&-\frac{1}{\Gamma_{\mu}}\left\langle K_{\mu}^{\dagger}\right\rangle^{(22\overline{1})}-i\left\langle C_{\mu}\right\rangle^{(22\overline{1})}, \qquad (3.125)
\end{aligned}
$$

where for a large system:

$$\begin{aligned}
\langle C_\mu \rangle^{(22\overline{1})} &= \frac{e^4 a_o^2 d^2}{\varepsilon_0 V \left|\mathbf{M}_o\right|^2 \hbar\omega_B}\Big(- \frac{\left(\chi_\parallel - 1\right)}{\left(\chi_\parallel + 1\right)} \sum_{\mu'\mu''\mu'''\mu''''\mu'''''} \widetilde{\mathbf{G}}_{\mu'',\mu'''}\widetilde{\mathbf{G}}_{\mu',\mu} \\
&\cdot Y^{\mu''',\mu'}_{\mu'''',\mu'''''} \left\langle K^\dagger_{\mu''} K^\dagger_{\mu'''',\mu'''''} K_{\mu''''} \right\rangle^{(22\overline{1})} e^{i\left(\widetilde{\omega}^0_{\mu''} + \widetilde{\omega}^0_{\mu'''',\mu'''''} - \widetilde{\omega}^0_{\mu} - \widetilde{\omega}^0_{\mu'''',\mu'''''}\right)\tau} \\
&+ \sum_{\mu'\mu''\mu'''\mu'''',\mu'''''} \{ \widetilde{\mathbf{G}}_{\mu'''',\mu'''''}\widetilde{\mathbf{G}}_{\mu'',\mu'} Y^{\mu',\mu}_{\mu''',\mu''''} \\
&\cdot \left\langle K^\dagger_{\mu''} K^\dagger_{\mu''',\mu'''''} K_{\mu''''} \right\rangle^{(22\overline{1})} e^{i\left(\widetilde{\omega}^0_{\mu''} + \widetilde{\omega}^0_{\mu''',\mu'''''} - \widetilde{\omega}^0_{\mu} - \widetilde{\omega}^0_{\mu'''',\mu'''''}\right)\tau} \\
&- \widetilde{\mathbf{G}}_{\mu'''',\mu''}\widetilde{\mathbf{G}}_{\mu'',\mu'} Y^{\mu',\mu}_{\mu''',\mu''''} \left\langle K^\dagger_{\mu'''',\mu'''''} K^\dagger_{\mu''',\mu''''} K_{\mu''''} \right\rangle^{(22\overline{1})} e^{i\left(\widetilde{\omega}^0_{\mu'''',\mu'''''} + \widetilde{\omega}^0_{\mu''',\mu''''} - \widetilde{\omega}^0_{\mu} - \widetilde{\omega}^0_{\mu''''}\right)\tau} \\
&- \widetilde{\mathbf{G}}_{\mu'''',\mu'''}\widetilde{\mathbf{G}}_{\mu'',\mu'} Y^{\mu',\mu}_{\mu''',\mu''''} \left\langle K^\dagger_{\mu'''',\mu'''''} K^\dagger_{\mu''} K_{\mu''''} \right\rangle^{(22\overline{1})} e^{i\left(\widetilde{\omega}^0_{\mu'''',\mu'''''} + \widetilde{\omega}^0_{\mu''} - \widetilde{\omega}^0_{\mu} - \widetilde{\omega}^0_{\mu''''}\right)\tau} \Big),
\end{aligned} \tag{3.126}$$

We can see that $\langle C_\mu \rangle^{(22\overline{1})} \tilde{} 1/V$ and therefore, in a large system, this contribution goes to zero, so in fact the third order equation becomes

$$\begin{aligned}
\frac{d\left\langle K^\dagger_\mu \right\rangle^{(22\overline{1})}}{d\tau} &= -\frac{1}{\Gamma_\mu}\left\langle K^\dagger_\mu \right\rangle^{(22\overline{1})} + i\frac{2ea_o\mathcal{E}^*_2(\tau/\omega_B)}{\hbar\omega_B} \\
&\cdot \sum_{\mu',\mu'',\mu'''} \widetilde{S}^*_{\mu'} Y^{\mu',\mu}_{\mu'',\mu'''} \left\langle K^\dagger_{\mu''} K_{\mu'''} \right\rangle^{(2\overline{1})} e^{i\left(\widetilde{\omega}_c - \widetilde{\omega}^0_\mu + \widetilde{\omega}^0_{\mu''} - \widetilde{\omega}^0_{\mu'''}\right)\tau} \\
&+ i\frac{ed\mathbf{E}_{\perp THz}}{\hbar\omega_B} \cdot [\sum_{\mu'} \widetilde{\mathbf{G}}_{\mu',\mu} \left\langle K^\dagger_{\mu'} \right\rangle^{(22\overline{1})} e^{i\left(\widetilde{\omega}^0_{\mu'} - \widetilde{\omega}^0_\mu\right)\tau} \\
&- 2\frac{e^2 a_o^2}{\left|\mathbf{M}_o\right|^2} \sum_{\mu'\mu''\mu'''\mu''''} \widetilde{\mathbf{G}}_{\mu'',\mu'} Y^{\mu',\mu}_{\mu''',\mu''''} \\
&\cdot \left\langle K^\dagger_{\mu''} K^\dagger_{\mu'''} K_{\mu''''} \right\rangle^{(22\overline{1})} e^{i\left(\widetilde{\omega}^0_{\mu''} + \widetilde{\omega}^0_{\mu'''} - \widetilde{\omega}^0_\mu - \widetilde{\omega}^0_{\mu''''}\right)\tau}] \\
&+ \frac{i}{\varepsilon_0\left(1+\chi_\parallel\right)} \frac{e^4 d}{\left|\mathbf{M}_o\right|^2 \hbar\omega_B} \sum_{\mu',\mu'',\mu'''} \widetilde{\mathbf{G}}_{\mu'',\mu'''} \\
&\cdot \widetilde{\mathbf{G}}_{\mu',\mu} \left\langle K^\dagger_{\mu''} K^\dagger_{\mu'} K_{\mu'''} \right\rangle^{(22\overline{1})} e^{i\left(\widetilde{\omega}^0_{\mu''} + \widetilde{\omega}^0_{\mu'} - \widetilde{\omega}^0_\mu - \widetilde{\omega}^0_{\mu'''}\right)\tau},
\end{aligned} \tag{3.127}$$

Finally, we have for the third-order DFWM intraband polarization:

$$\langle \mathbf{P}_{inter} \rangle^{(22\overline{1})} = \frac{2e}{da_o} \operatorname{Re}\left\{ \sum_\mu \widetilde{S}_\mu \left\langle K^\dagger_\mu \right\rangle^{(22\overline{1})} e^{i\omega^0_\mu t} \right\}. \tag{3.128}$$

3.6 Equations of motion using Factoring

A simplified set of equations can be obtained if one is willing to simply factor the above third order equation. If we assume that we can write

$$\left\langle K^{\dagger}_{\mu''}K^{\dagger}_{\mu'''}K_{\mu''''}\right\rangle^{(22\bar{1})} = \left\langle K^{\dagger}_{\mu''}\right\rangle^{(2)}\left\langle K^{\dagger}_{\mu'''}K_{\mu''''}\right\rangle^{(2\bar{1})}, \tag{3.129}$$

then we obtain the following equations of motion:

$$\begin{aligned}\frac{d\left\langle K_{\mu}\right\rangle^{(\bar{1})}}{d\tau}+\frac{1}{\Gamma_{\mu}}\left\langle K_{\mu}\right\rangle^{(\bar{1})} &= i\mathcal{E}_1(\tau/\omega_B)e^{-i\left(\widetilde{\omega}_c-\widetilde{\omega}^0_{\mu}\right)\tau}\cdot\widetilde{S}_{\mu}\frac{|\mathbf{M}_o|^2}{a_o\hbar\omega_B}\\ &\quad -i\frac{d\mathbf{E}_{THz}}{\hbar\omega_B}\cdot\sum_{\mu'}\widetilde{\mathbf{G}}^{*}_{\mu',\mu}\left\langle K_{\mu'}\right\rangle^{(\bar{1})}e^{-i\left(\widetilde{\omega}^0_{\mu'}-\widetilde{\omega}^0_{\mu}\right)\tau}, \qquad (3.130)\\ \frac{d\left\langle K^{\dagger}_{\mu}\right\rangle^{(2)}}{d\tau}+\frac{1}{\Gamma_{\mu}}\left\langle K^{\dagger}_{\mu}\right\rangle^{(2)} &= -i\mathcal{E}^{*}_2(\tau/\omega_B)e^{i\left(\widetilde{\omega}_c-\widetilde{\omega}^0_{\mu}\right)\tau}\cdot\widetilde{S}_{\mu}\frac{|\mathbf{M}_o|^2}{a_o\hbar\omega_B}\\ &\quad +i\frac{d\mathbf{E}_{THz}}{\hbar\omega_B}\cdot\sum_{\mu'}\widetilde{\mathbf{G}}_{\mu',\mu}\left\langle K^{\dagger}_{\mu'}\right\rangle^{(2)}e^{i\left(\widetilde{\omega}^0_{\mu'}-\widetilde{\omega}^0_{\mu}\right)\tau}, \qquad (3.131)\end{aligned}$$

$$\begin{aligned}\frac{d\left\langle K^{\dagger}_{\mu}K_{\nu}\right\rangle^{(2\bar{1})}}{d\tau} &= -\frac{1}{\Gamma_{\mu\nu}}\left\langle K^{\dagger}_{\mu}K_{\nu}\right\rangle^{(2\bar{1})}+-i\mathcal{E}^{*}_2(\tau/\omega_B)e^{i\left(\widetilde{\omega}_c-\widetilde{\omega}^0_{\mu}\right)\tau}\cdot\widetilde{S}^{*}_{\mu}\frac{|\mathbf{M}_o|^2}{a_oe\hbar\omega_B}\left\langle K_{\nu}\right\rangle^{(\bar{1})}\\ &\quad +i\mathcal{E}_1(\tau/\omega_B)e^{i\left(-\widetilde{\omega}_c+\widetilde{\omega}^0_{\nu}\right)\tau}\cdot\widetilde{S}_{\nu}\frac{|\mathbf{M}_o|^2}{a_oe\hbar\omega_B}\left\langle K^{\dagger}_{\mu}\right\rangle^{(2)}\\ &\quad +i\frac{ed\mathbf{E}_{\perp THz}}{\hbar\omega_B}\cdot\sum_{\mu'}(\widetilde{\mathbf{G}}_{\mu',\mu}\left\langle K^{\dagger}_{\mu'}K_{\nu}\right\rangle^{(2\bar{1})}e^{i\left(\widetilde{\omega}^0_{\mu'}-\widetilde{\omega}^0_{\mu}\right)\tau}\\ &\quad -\widetilde{\mathbf{G}}^{*}_{\mu',\nu}\left\langle K^{\dagger}_{\mu}K_{\mu'}\right\rangle^{(2\bar{1})}e^{-i\left(\widetilde{\omega}^0_{\mu'}-\widetilde{\omega}^0_{\nu}\right)\tau}), \qquad (3.132)\end{aligned}$$

$$
\begin{aligned}
\frac{d\left\langle K_{\mu}^{\dagger}\right\rangle^{(22\overline{1})}}{d\tau} &= -\frac{1}{\Gamma_{\mu}}\left\langle K_{\mu}^{\dagger}\right\rangle^{(22\overline{1})}+i\frac{2ea_{o}\mathcal{E}_{2}^{*}(\tau/\omega_{B})}{\hbar\omega_{B}} \\
&\cdot\sum_{\mu',\mu'',\mu'''}\widetilde{S}_{\mu'}^{*}Y_{\mu'',\mu'''}^{\mu',\mu}\left\langle K_{\mu''}^{\dagger}K_{\mu'''}\right\rangle^{(2\overline{1})}e^{i\left(\widetilde{\omega}_{c}-\widetilde{\omega}_{\mu}^{0}+\widetilde{\omega}_{\mu''}^{0}-\widetilde{\omega}_{\mu'''}^{0}\right)\tau} \\
&+i\frac{ed\mathbf{E}_{\perp THz}}{\hbar\omega_{B}}\cdot[\sum_{\mu'}\widetilde{\mathbf{G}}_{\mu',\mu}\left\langle K_{\mu'}^{\dagger}\right\rangle^{(22\overline{1})}e^{i\left(\widetilde{\omega}_{\mu'}^{0}-\widetilde{\omega}_{\mu}^{0}\right)\tau} \\
&-2\frac{e^{2}a_{o}^{2}}{\left|\mathbf{M}_{o}\right|^{2}}\sum_{\mu'\mu''\mu'''\mu''''}\widetilde{\mathbf{G}}_{\mu'',\mu'}Y_{\mu''',\mu''''}^{\mu',\mu} \\
&\cdot\left\langle K_{\mu''}^{\dagger}\right\rangle^{(2)}\left\langle K_{\mu'''}^{\dagger}K_{\mu''''}\right\rangle^{(2\overline{1})}e^{i\left(\widetilde{\omega}_{\mu''}^{0}+\widetilde{\omega}_{\mu'''}^{0}-\widetilde{\omega}_{\mu}^{0}-\widetilde{\omega}_{\mu''''}^{0}\right)\tau}] \\
&+\frac{i}{\varepsilon_{0}\left(1+\chi_{\parallel}\right)}\frac{e^{4}d}{\left|\mathbf{M}_{o}\right|^{2}\hbar\omega_{B}}\left[\sum_{\mu'',\mu'''}\widetilde{\mathbf{G}}_{\mu'',\mu'''}\left\langle K_{\mu''}^{\dagger}K_{\mu'''}\right\rangle^{(2\overline{1})}e^{i\left(\widetilde{\omega}_{\mu''}^{0}-\widetilde{\omega}_{\mu'''}^{0}\right)\tau}\right] \\
&\cdot\left[\sum_{\mu'}\widetilde{\mathbf{G}}_{\mu',\mu}\left\langle K_{\mu'}^{\dagger}\right\rangle^{(2)}e^{i\left(\widetilde{\omega}_{\mu'}^{0}-\widetilde{\omega}_{\mu}^{0}\right)\tau}\right], \qquad (3.133)
\end{aligned}
$$

Note that the last term in the third-order equation factors into the intraband polarization times the usual THz dipole factor. Note that there are now two fewer equations, as the second order equation $\left\langle K_{\mu}^{\dagger}K_{\nu}^{\dagger}\right\rangle^{(22)}$, (3.123), was only required in the calculation of $\left\langle K_{\mu''}^{\dagger}K_{\mu'''}^{\dagger}K_{\mu''''}\right\rangle^{(22\overline{1})}$,(3.124).

This factorization is physically reasonable as it allows one to more readily see the driving forces behind the third order polarization, the intraband polarization, and the THz field created by the exciton dipoles. In our system of equations, $\left\langle K_{\mu''}^{\dagger}\right\rangle^{(2)}$ represents the creation of excitons due to the optical field, while $\left\langle K_{\mu'''}^{\dagger}K_{\mu''''}\right\rangle^{(2\overline{1})}$ indicates that an exciton with an electron-hole separation denoted by μ'''' is destroyed, and another, with its separation indicated by μ''' is created. This can also represent a change in a given exciton's electron-hole separation, from μ'''' to μ'''. $\left\langle K_{\mu''}^{\dagger}K_{\mu'''}^{\dagger}K_{\mu''''}\right\rangle^{(22\overline{1})}$, representing the destruction of one exciton and the creation of two more, has no real equivalent in terms of a physical process to support it, even though it is important to the evolution of $\left\langle K_{\mu}^{\dagger}\right\rangle^{(22\overline{1})}$ in the full system of equations. Thus, from a physical standpoint, it is reasonable to factor the third order term into two parts.

Chapter 4

Results and Discussion

In this chapter, we examine the results of the calculations done. We deal with the calculation of $X^{\mu,\mu'}_{\mu'',\mu'''}$, and its effects on the overall DFWM intensity. We then examine the results obtained via the full system of equations, and compare them to other experimental results. At this point, we then compare the factorized version of our system of equations to the full system, in order to determine whether the factorization is a valid one. First, however, we will detail the parameters of the superlattice which we modeled for this calculation.

The superlattice modeled consists of 21 periods of 84 angstroms each, and is subjected to a static field of 15 kV/cm, for an eFd value of 12.6 meV. The exciting laser pulses were set to a point midway between the $p = 0$ and $p = -1$ transitions for this superlattice, at an energy of 62 meV. They were modeled as Gaussians with a width of 1.47. The field strength associated with the two pulses was 1.9 MV/m, and the relative phase between them was set to be 0. The inplane masses of the electrons and holes were 0.0665 and 0.115 m_e, respectively, where m_e is the mass of an electron. The dielectric constant of the SL was set as 12.5. The energy gap between the conduction and valence band was 1.52 eV. The interband dephasing time was set to be 10, the intraband dephasing time as 15. For the unfactored version, the dephasing time associated with $\left\langle K^{\dagger}_{\mu} K^{\dagger}_{\mu'} \right\rangle^{(22)}$ was 5. For the third order equation, $\left\langle K^{\dagger}_{\mu''} K^{\dagger}_{\mu'} K_{\mu'''} \right\rangle^{(22\overline{1})}$, the dephasing times were 10 for the diagonal elements, and 6 for non-diagonal ones. All these times are in units of $1/\omega_B$.

4.1 $X^{\mu,\mu'}_{\mu'',\mu'''}$.for the 1s Exciton

As was discussed in the previous chapter, $X^{\mu,\mu'}_{\mu'',\mu'''}$ is given by the following for 1s excitons.

$$\chi^{\mu,\mu'}_{\mu'',\mu'''} = \frac{16\pi}{AN_z} \sum_{l,l'} D^{\mu *}_{l} D^{\mu'''}_{l} D^{\mu'}_{l'} D^{\mu'' *}_{l'} \cdot F\left(\lambda_\ell, \lambda_{\ell'}\right) \tag{4.1}$$

These X parameters describe phase-space filling. This reflects how much of the superlattice volume actually contains excitons. In Figure 4-1, we have plotted $X^{\mu,\mu'}_{\mu'',\mu'''}$, with $\mu = \mu'''$, and $\mu' = \mu''$. This was done for a system with 41 states. One can readily see that the value of $X^{\mu,\mu'}_{\mu'',\mu'''}$ increases rapidly as either pair of coefficients moves away from the central value of 0. This is due to the weaker binding of these states, which leads to them being more localized in phase space. This causes them to block phase space more effectively then their less localized counterparts. It is therefore expected that phase-space filling be more important for those states which undergo excited in-plane motion than for the 1s states studied here. This should be kept in mind for any calculation involving these states. Also, $X^{\mu,\mu'}_{\mu'',\mu'''}$ is symmetric about the line where all four indices are equal, i.e., the value of $X^{\mu,\mu'}_{\mu'',\mu'''}$ is unchanged if these two pairs are interchanged, i.e.,$X^{2,1}_{1,2} = X^{1,2}_{2,1}$. This is due to the fact that $F\left(\lambda_\ell, \lambda_{\ell'}\right)$ is equal to $F\left(\lambda_{\ell'}, \lambda_{\ell}\right)$. If the indices ℓ and ℓ' are switched around in equation (3.63), you can see that the numerator and the first term of the denominator have their signs reversed, whereas the second term remains unchanged.

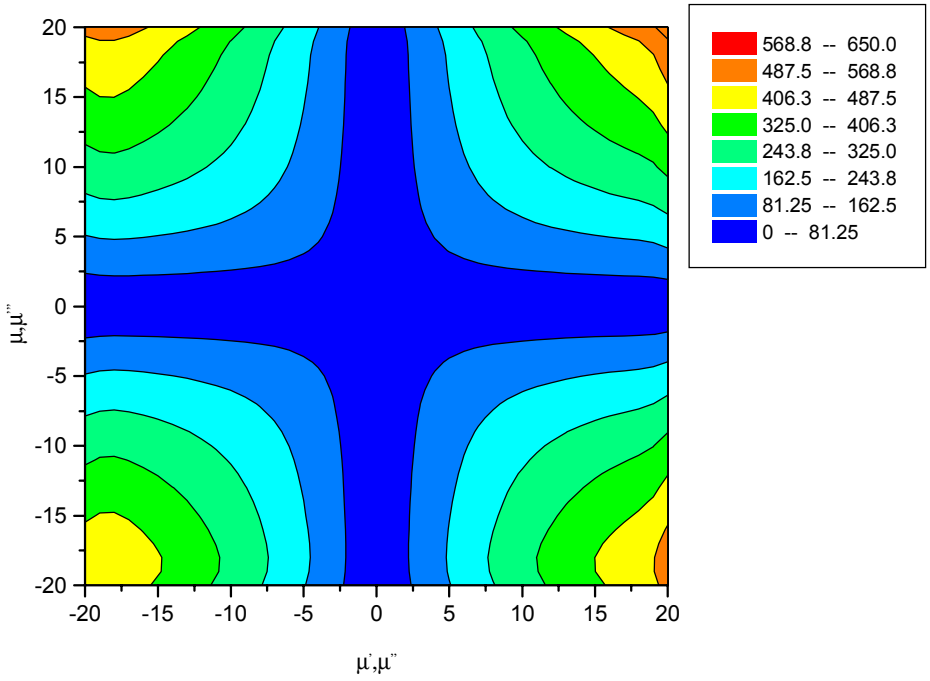

Figure 4-1: A plot of $X^{\mu,\mu'}_{\mu'',\mu'''}$ for a 41 state system, where $\mu = \mu'''$, and $\mu' = \mu''$.

4.2 The Importance of Phase Space Filling

The equation of motion for $\left\langle K^{\dagger}_{\mu} \right\rangle^{(22\overline{1})}$ has several terms in it. The second term, shown below, is referred to as the phase-space filling term, because it is the only one which contains $Y^{\mu,\mu'}_{\mu'',\mu'''}$, which is directly related to $X^{\mu,\mu'}_{\mu'',\mu'''}$ by equation (**??**).

$$i\frac{2ea_o\mathcal{E}^*_2(\tau/\omega_B)}{\hbar\omega_B}\cdot\sum_{\mu',\mu'',\mu'''}\widetilde{S}^*_{\mu'}Y^{\mu',\mu}_{\mu'',\mu'''}\left\langle K^{\dagger}_{\mu''}K_{\mu'''}\right\rangle^{(2\overline{1})}e^{i\left(\widetilde{\omega}_c-\widetilde{\omega}^0_{\mu}+\widetilde{\omega}^0_{\mu''}-\widetilde{\omega}^0_{\mu'''}\right)\tau} \tag{4.2}$$

When these equations are solved numerically, it is found that this term is significantly smaller than the other terms in the equation. The following series of graphs, Figure 4-2, show the absolute differences between the values obtained with $Y^{\mu,\mu'}_{\mu'',\mu'''}$ included, and without, normalized to the average intensity of the DFWM signal. They are plotted for several different pulse time delays. They all reveal a similar occurrence. There is a very tiny difference immediately at the beginning of the second pulse, and then the two are identical. As you can see by the amplitude

of the normalized 'spike', the difference is very small in comparison to the signal strength, the largest being 13 orders of magnitude smaller than that of the signals it arises from. This shows that the phase-space filling term has a negligible effect on the intensity of the signal, and can be safely removed without any loss of accuracy. This is due to the fact that the exciton density in the superlattice is quite small. From basic EM theory, we can write that $P = \varepsilon\epsilon_0 E$, where P is the polarization caused by a given electric field, E. ε is the dielectric constant for the material. We can replace P by Np/V, where p is the dipole moment associated with one exciton, ed. Putting these together gives

$$\frac{N}{V} = \frac{\varepsilon\epsilon_0 E}{ed} \tag{4.3}$$

Substituting in the values associated with the modeled superlattice gives an exciton density of $1.23 * 10^{23}$ excitons/m^3. This seems like quite a lot. However, if we multiply the volume of an exciton, given by da_0^2, by this figure, we will arrive at the actual ratio of the total volume in the superlattice to that volume occupied by excitons. The volume of the excitons is $2.35*10^{-29}$ m^3. This yields a ratio of $2.90*10^{-6}$. For every million excitons which could fit into a given volume, we only have three. It should also be noted that the removing of the phase space filling term increased the speed of calculation by a significant factor, as the number of iterations needed to calculate this term rises as the number of states to the fourth power.

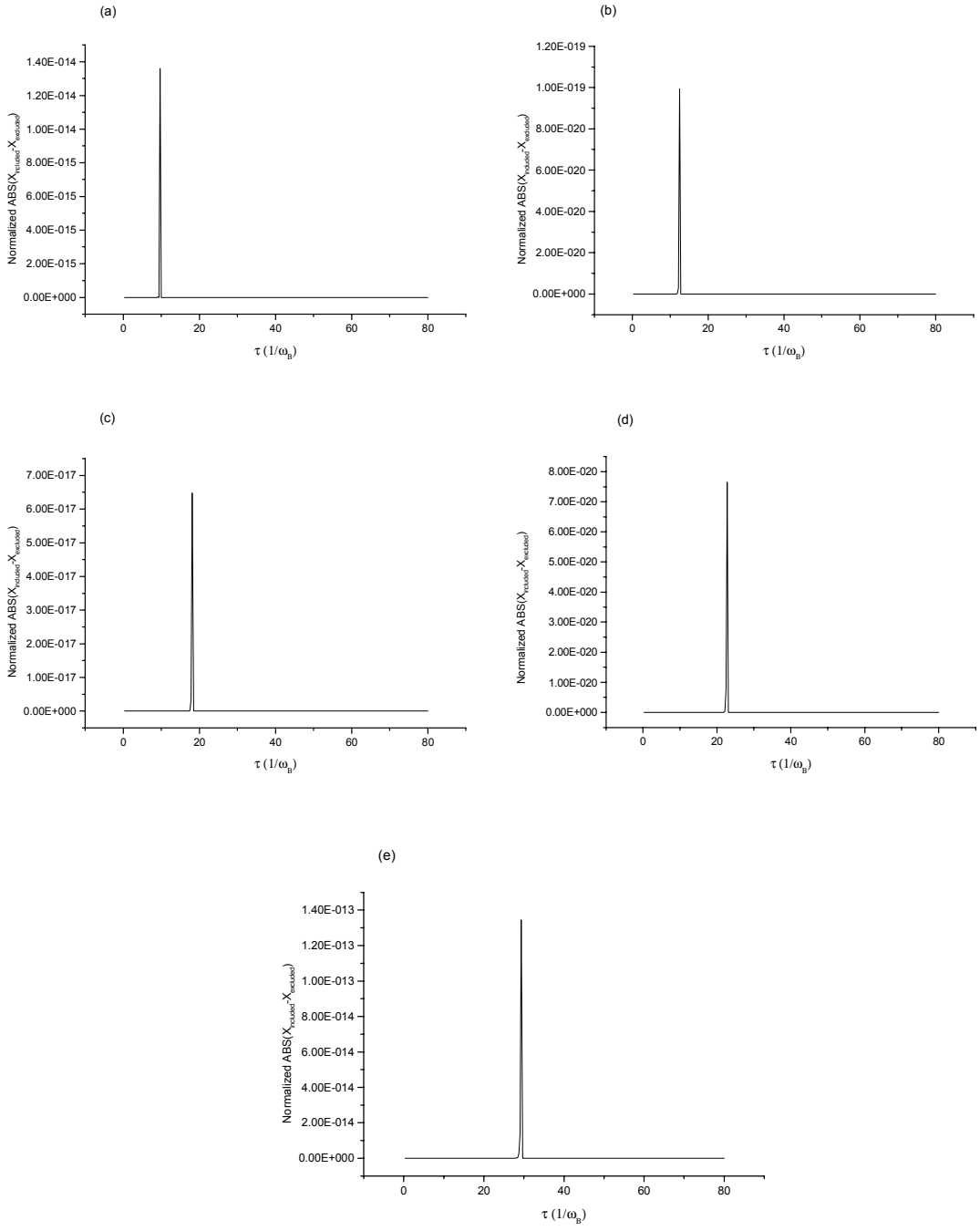

Figure 4-2: Differences in calculated DFWM signal between calculations done with phase-space filling included, and without. These were done for pulse time delays of: (a) 0, (b) 5, (c) 10, (d) 15, and (e) 20, where time is in units of $1/\omega_B$.

4.3 Results of the Full System of equations

In this section, we will analyze the results obtained via the full system of equations. We will look at the spectral power density of the system and the absorption spectrum associated with the modeled superlattice. We will then examine the time evolution of $\left\langle K_\mu^\dagger \right\rangle^{(22\overline{1})}$ via Time-Resolved DFWM spectra. Finally, we will show the Time-Integrated DFWM plot.

4.3.1 Third Order Spectral Power Density

The plot below, Figure 4-3, shows the spectral power density for our system for several pulse delays. You can see 6 peaks here, each approximately a distance of ω_B apart. Each of these is associated with an excitonic peak with a different electron-hole separation. Also, the power density drops as the time delay between the two pulses increases. You can also see that the peaks do not shift in frequency as the time delay changes. This is to be expected, as our calculations are only done to third order, and the oscillation of the peak frequencies is a phenomenon which is observed only when higher order calculations are performed. If we look at the equations (3.109) and (3.108), we see that $\left\langle B_\mu^\dagger \right\rangle^{(22\overline{1})}$ has a natural frequency given by ω_μ^0. However, it is being driven by the $\left\langle B_\mu^\dagger B_{\mu'}^\dagger B_{\mu''} \right\rangle^{(22\overline{1})}$ at a frequency given by $-\left(\hbar\omega_{\mu''}^0 - \hbar\omega_{\mu'}^0 - \hbar\omega_\mu^0\right)$. If we treat the excitons as driven oscillators, the they can only oscillate at one of these two frequencies. In order for there to be oscillations of these frequencies, they must be associated with an exciting field, in order to gain a dependance on the pulse time delay. If we associate a electric field with the $\left\langle B_\mu^\dagger \right\rangle^{(22\overline{1})}$ terms to examine these effects, we get terms which are higher than third order.

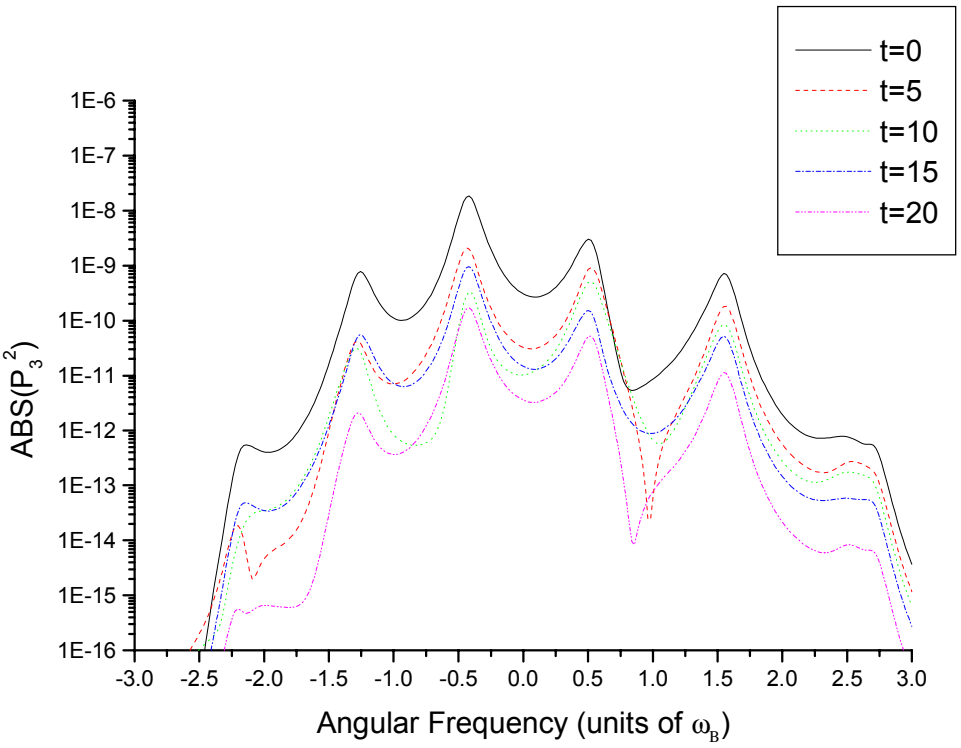

Figure 4-3: Power spectrum calculated for the modeled superlattice

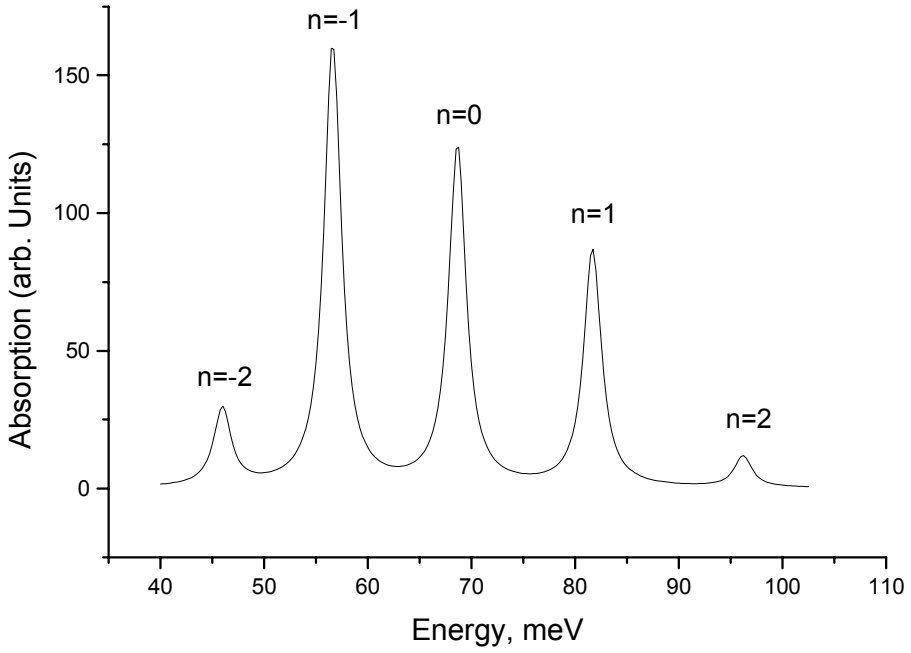

Figure 4-1: Figure 4-4: Absorption spectra as a function of energy for a superlattice. The central frequency of the laser is at 62 meV.

4.3.2 Absorption

Figure 4-4 shows the calculated absorption as a function of energy for the superlattice structure described at the beginning of the chapter. This gives identical results to the exciton curve in Figure 1 in Dignam[35]. Each peak represents the absorption energy associated with a specific exciton state. You can see that the excitonic WSL energy spacings, given by the distance between two adjacent peaks, are not equal. This is due to the electron-hole binding energy for that state, i.e., that particular electron-hole separation distance (nd). This has the effect of causing the energy spacings to increase as the WSL index increases.

4.3.3 Time-Integrated DFWM signal for the modeled SL

In Figure 4-5, the TIDFWM signal is plotted versus pulse time delay for the superlattice modeled. This is the same as was plotted by Feldmann et al. 2-6[3]. You can see two peaks after the initial decay, at time delays of ~7 and 14. These correspond to time delays of 0.37 and 0.73 ps, respectively. These peaks represent when Bloch oscillations occur. At these delay times, the electron is able to traverse the entire Brillouin zone and return to it's initial state during the time between the first and second pulse. The Bloch oscillation period obtained via equation (2.26) is equal to 0.34 ps, which is in good agreement with our calculated results.

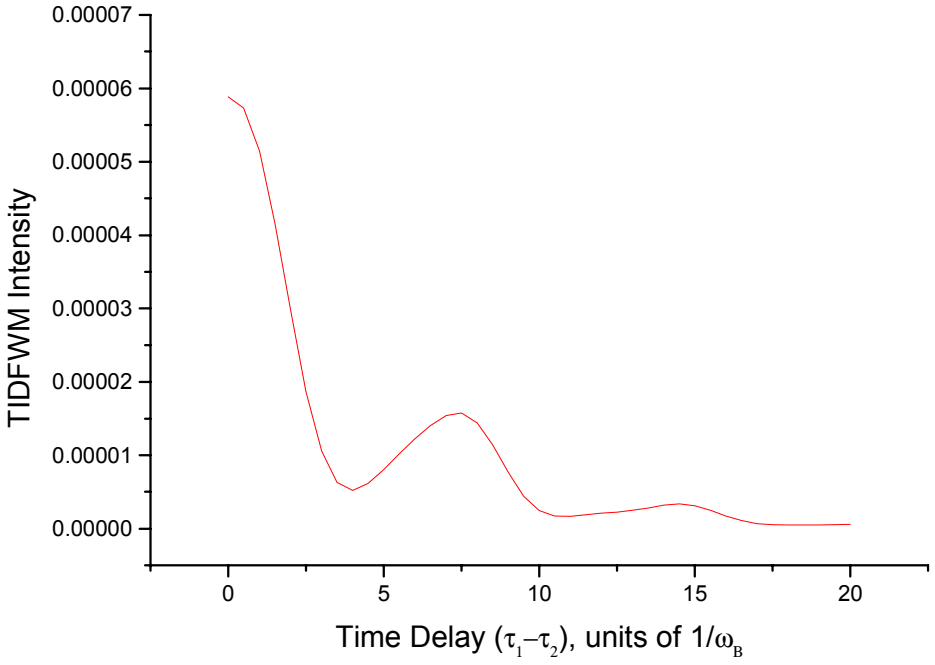

Figure 4-5: TIDFWM signal as a function of pulse time delay for $eFd = 6.2$ meV.

4.3.4 Time Evolution of $\left\langle K_{\mu}^{\dagger} \right\rangle^{(22\bar{1})}$

In Figure 4-6, The Time-Resolved DFWM signal is plotted as a function of time. This is done for several different pulse time delays, ranging from $\tau_1 - \tau_2 = -10$ to $\tau_1 - \tau_2 = 20$, where the times are given in units of $1/\omega_B$. You can see that in each case, there are a number of oscillations, which occur at more than one frequency. These are due to beating between the frequencies associated with each excitonic state. It should also be noted that each of these double peaks occurs at intervals of approximately 7 time units, which corresponds to the Bloch

oscillation time observed in the previous section. Also, the amplitude of the signal drops off as the absolute value of the time delay increases. This is due to increased dephasing of the polarization induced in the superlattice by the first pulse as the time delay between the two pulses increases.

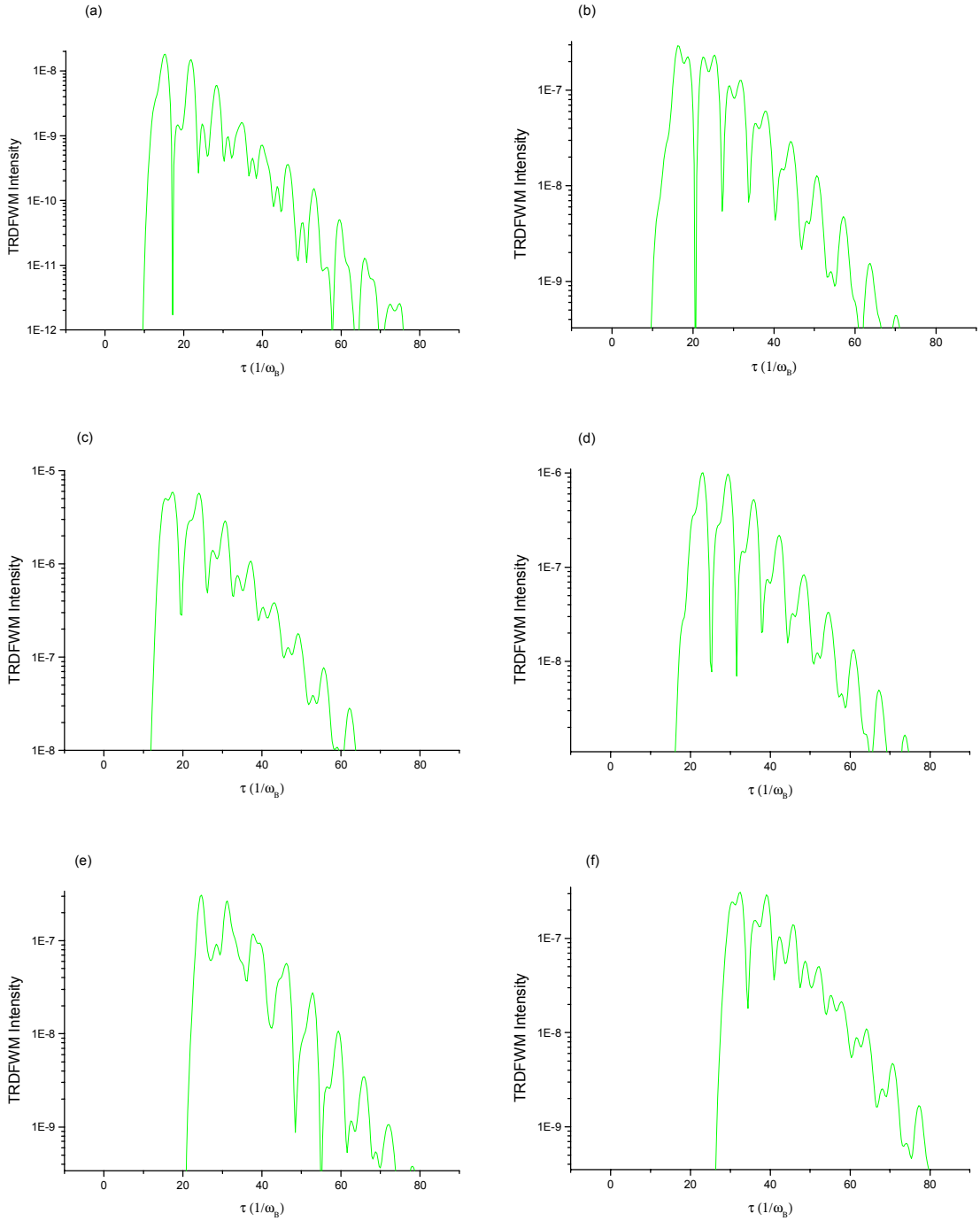

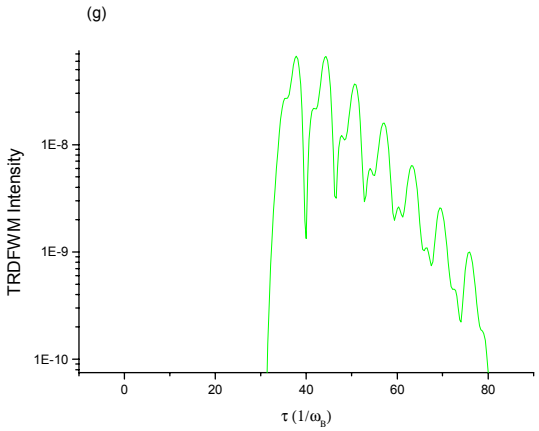

Figure 4-6: Logarithmic plots of the time evolution of the Time-Resolved DFWM signal, These are done for seven different pulse time delays, which are: (a) -10, (b) -5, (c) 0, (d) 5, (e) 10, (f) 15, and (g) 20 . All times are in units of $1/\omega_B$.

4.4 Comparing The Factored and Unfactored Versions

In the previous chapter, we created a simplified version of the system of equations by factoring the third order term $\left\langle K^\dagger_{\mu''} K^\dagger_{\mu'} K_{\mu'''} \right\rangle^{(22\overline{1})}$ into a product of a first and second order term, using the following:

$$\left\langle K^\dagger_{\mu} K^\dagger_{\mu'} K_{\mu''} \right\rangle^{(22\overline{1})} = \left\langle K^\dagger_{\mu} \right\rangle^{(2)} \left\langle K^\dagger_{\mu'} K_{\mu''} \right\rangle^{(2\overline{1})}. \tag{4.4}$$

By using this factorization, we were able to remove the need for two of the equations in the system: $\left\langle K^\dagger_{\mu''} K^\dagger_{\mu'} K_{\mu'''} \right\rangle^{(22\overline{1})}$, equation (3.124), as well as $\left\langle K^\dagger_{\mu} K^\dagger_{\mu'} \right\rangle^{(22)}$, equation (3.123). This section deals with the validity of this approximation.

The following series of graphs, Figure 4-7, shows logarithmic plots of the Time-Resolved Degenerate Four-Wave Mixing intensity (TRDFWM) for seven different time delays, ranging from $\tau_1 - \tau_2 = -10$ to $\tau_1 - \tau_2 = 20$, where the times are given in units of $1/\omega_B$. As you can see, there is good agreement between the factored and unfactored results in all cases. The factored system of equations seems to lead to smaller predictions than the unfactored version, however, the shape of the curves is the same in all cases except for the time delay of 10.

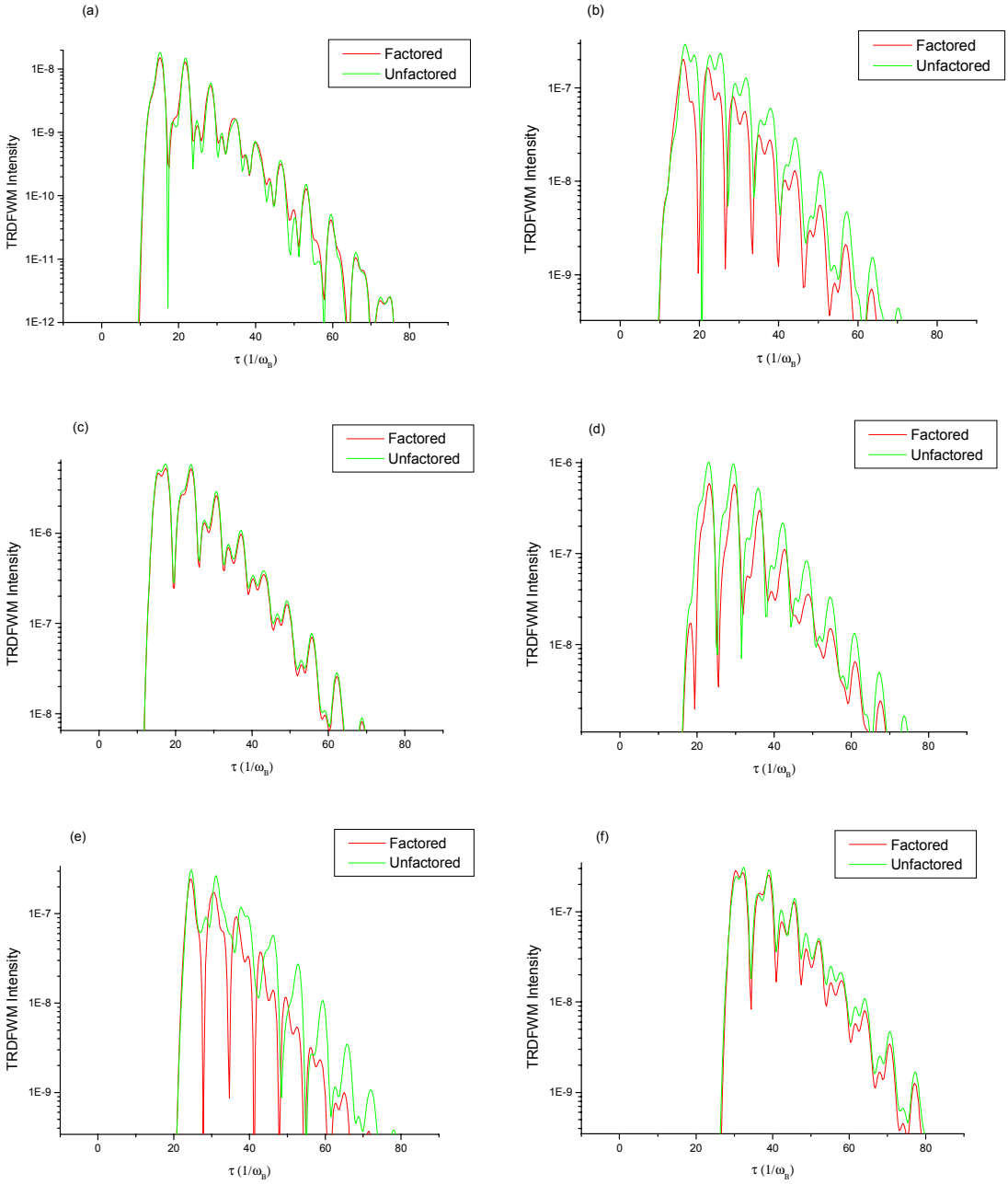
(a)
Factored
Unfactored
TRDFWM Intensity
1E-8
1E-9
1E-10
1E-11
1E-12
0
20
40
60
80
τ (1/ω_B)
(b)
Factored
Unfactored
TRDFWM Intensity
1E-7
1E-8
1E-9
0
20
40
60
80
τ (1/ω_B)
(c)
Factored
Unfactored
TRDFWM Intensity
1E-6
1E-7
1E-8
0
20
40
60
80
τ (1/ω_B)
(d)
Factored
Unfactored
TRDFWM Intensity
1E-6
1E-7
1E-8
0
20
40
60
80
τ (1/ω_B)
(e)
Factored
Unfactored
TRDFWM Intensity
1E-7
1E-8
1E-9
0
20
40
60
80
τ (1/ω_B)
(f)
Factored
Unfactored
TRDFWM Intensity
1E-7
1E-8
1E-9
0
20
40
60
80
τ (1/ω_B)

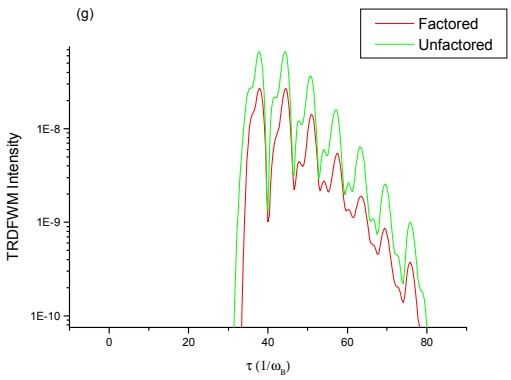

Figure 4-7: Logarithmic plots of the Time-Resolved DFWM signal, showing the difference between the factored and unfactored system of equations. These are done for seven different pulse time delays, which are: (a) -10, (b) -5, (c) 0, (d) 5, (e) 10, (f) 15, and (g) 20 . All times are in units of $1/\omega_B$

Figure 4-8 shows the Time-Integrated Four-Wave Mixing intensity for both the factored and unfactored versions plotted against time delay. Again, you can see that there is good agreement between the two versions.

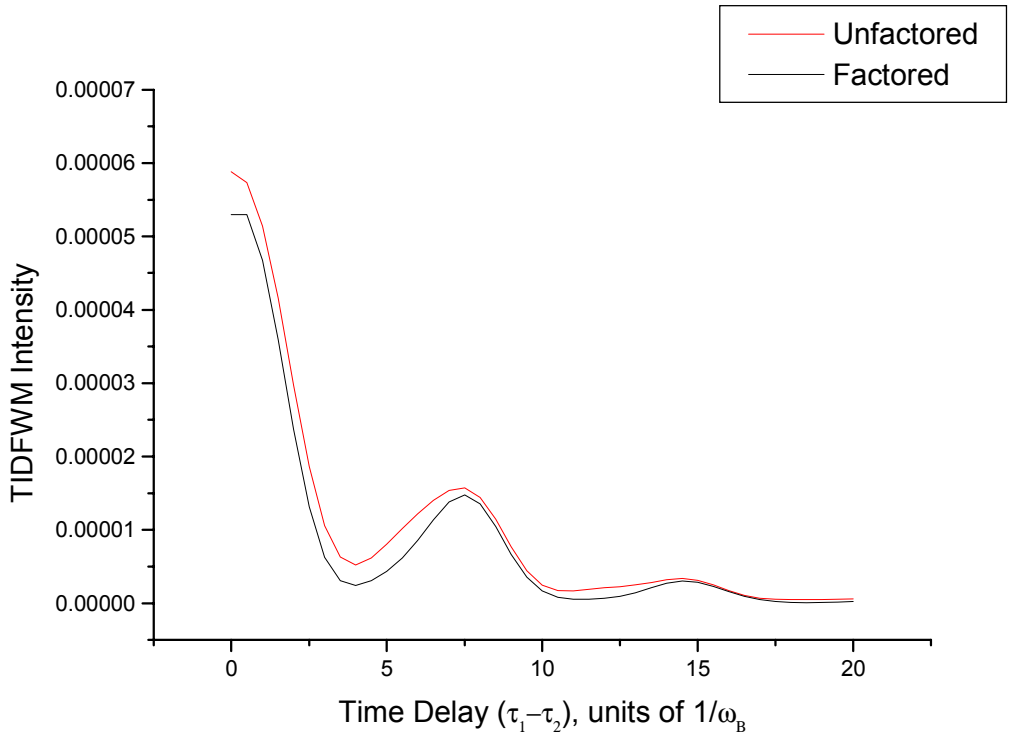

Figure 4-8: Comparison of Time-integrated DFWM signals for the factored and unfactored versions of the system of equations.

It should also be noted that using the factored version significantly speeds up the time required to perform a calculation, since the two equations which are removed are two of the four higher order equations.

Chapter 5

Summary

In this thesis we developed the first numerical calculation of Degenerate Four-Wave Mixing in a biased Semiconductor Superlattice. This calculation was done to third order in the electric field using an exciton basis.

We found that the effects of phase-space filling on the calculated DFWM signal are negligible. A calculation done without the phase-space filling terms showed only an very tiny difference when compared to the calculation done with the phase-space filling terms included. This difference occurred at the onset of the second pulse, and aside from this discrepancy, the two versions were identical. The size of the largest difference, after normalizing to the average DFWM signal, was on the order of 10^{-13}. This was due to the fact that the density of electrons was insufficient for phase-space filling to become a significant factor. This allowed us to remove the phase-space filling term from the system of equations entirely.

An examination of the spectral power density showed several peaks associated with excitons of various electron-hole separations. The frequencies associated with these peaks were stationary with respect to the pulse time delay, because in order to model those effects in a third order calculation, the terms required are actually fifth order, and those terms were dropped.

The calculated absorption spectra showed good agreement with those calculated by Dignam[35]. They showed variations in the WSL energy spacings caused by the different binding energies associated with the different exciton states.

We also presented a factored version of the system of equations used. This was created by factoring the terms to third order in the electric field into a product of a first and second

order term. In doing this, we were able to reduce the number of equations needed to calculate $\left\langle K_{\mu}^{\dagger} \right\rangle^{(22\overline{1})}$ from six to four, by removing the third order equation, and one of the second order ones. We then compared this factorized version to the original, and found that they produced similar results.

5.1 Recommendations for further Study

In the program used to calculate the third-order DFWM, provision is made for the superlattice to be subjected to a THz field, in addition to the static electric field. An obvious course would be to examine the effects of the THz field on the results obtained, in order to determine if our formulism holds up under those circumstances.

Bibliography

[1] K. Leo, T.C. Damen, J. Shah, E. O. Göbel, and K. Köhler, Appl. Phys. Lett. **57,** 19 (1990).

[2] K. Leo,J. Shah, E. O. Göbel, T.C. Damen, S. Schmitt-Rink, W. Schäfer and K. Köhler, Phys. Rev. Lett. **66**, 201 (1991).

[3] J. Feldmann, K. Leo, J. Shah, D. A. B. Miller, J. E. Cunningham, T. Meier, G. von Plessen, A. Schulze, P. Thomas, and S. Schmitt-Rink, Phys. Rev. B **46**, 7252 (1992).

[4] C. Waschke, H. G. Roskos, R. Schwedler, K. Leo, H. Kurz, and K. Köhler, Phys. Rev. Lett. **70**, 3319 (1993).

[5] S. Schmitt-Rink, D. S. Chemla, Phys. Rev. Lett. **57**, 2752 (1986).

[6] See *e.g.,* H. Haug and S. W. Koch, *Quantum Theory of the Optical and Electronic Properties of Semiconductors* (World Scientific, Singapore, 1994), Third Edition.

[7] K. Victor, V. M. Axt, and A. Stahl, Phys. Rev. B **51**, 14164 (1995).

[8] V. M. Axt, G. Bartels, and A. Stahl, Phys. Rev. Lett. **76**, 2543 (1996).

[9] Margaret Hawton and Delene Nelson, Phys. Rev. B **57**, 4000 (1998).

[10] P. H. Bolivar, F. Wolter, A. Müller, H. G. Roskos, and H. Kurz, Phys. Rev. Lett. **78**, 2232 (1997).

[11] J.M. Lachaine, M. Hawton, and M.M. Dignam, to be published.

[12] H.M. James, Phys. Rev. **76,** 1611 (1949).

[13] E.O. Kane, J. Phys. Chem. Solids **12**, 181 (1959).

[14] G. H. Wannier, Phys. Rev. **117**, 432 (1969).

[15] P. W. A. Mcllroy, J. Appl. Phys. **59**, 3532 (1986).

[16] J. Bleuse, G. Bastard, and P. Voisin, Phys. Rev. Lett. **60,** 220 (1988).

[17] E. E. Mendez, F. Agulló-Rueda, and J. M. Hong, Phys. Rev. Lett. **60**, 2426 (1988).

[18] P. Voisin, J. Bleuse, C. Bouche, S. Gaillard, C. Alibert, and A. Regreny, Phys. Rev. Lett. **61**, 1639 (1988).

[19] R. Ferriera and G. Bastard, Phys. Rev. B **40,** 1074 (1989).

[20] M. Helm, P. England, E. Colas, F. de Rosa, and S.J. Allen, Phys Rev. Lett. **63,** 74 (1989).

[21] D. Bertram, H. Lage, H.T. Grahn, and K. Ploog, Appl. Phys. Lett. **64,** 1012 (1994).

[22] H. T. Grahn, *Semiconductor Superlattices: Growth and Electronic Properties*, (World Scientific Publishing Co. Pte. Ltd., 1995).

[23] M. M. Dignam, and J. E. Sipe, Phys. Rev. Lett. **64**, 1797 (1990).

[24] F. Bloch, Z. Phys. **52**, 555 (1928).

[25] F. Beltram, F. Capasso, D.L. Sivco, A.L. Hutchinson, S. Chu, and A.Y. Cho, Phys Rev. Lett. **64**, 3167 (1990).

[26] M. Dignam, J. E. Sipe, and J. Shah, Phys. Rev. B **49**, 10502 (1994).

[27] K. Leo, P. Haring Bolivar, F. Brüggemann, R. Schwedler, and K.Köhler, Solid State Comm. **84**, 943 (1992).

[28] P. Liesching, P. H. Bolivar, W.Beck, Y.Dhaibi, F. Brüggemann, R. Schwedler, H Kurz, K. Leo, and K. Köhler, Phys. Rev. **B50,** 14389 (1994).

[29] P. Leisching, W. Beck, H. Kurz, W. Schäfer, K. Leo, and K. Köhler, Phys Rev. **B51,** 7962 (1995).

[30] M. Sudzius, V. G. Lyssenko, F. Löser, K. Leo, M. M. Dignam, and K. Köhler, Phys. Rev. **B57**, 12693 (1998).

[31] F. Löser, Yu. A. Kosevich, K. Köhler, and K. Leo, Phys Rev **B61**, 13373 (2000).

[32] M. M. Dignam, and J. E. Sipe, Phys. Rev. **B41**, 2865 (1990).

[33] M. M. Dignam, and J. E. Sipe, Phys. Rev**. B43,** 4097 (1991).

[34] M. Hawton and M. M. Dignam, to be published.

[35] T. Usui, Prog. Theor. Phys. **23**, 787 (1960).

[36] N. W. Ashcroft and N. D. Mermin, *Solid State Physics* (Holt, Rinehart, and Winston, Philadelphia, 1976).

[37] C. Preister, G. Allan, and M. Lannoo, Phys Rev. **B 30,** 7302 (1984).

[38] M. M. Dignam, Phys. Rev. **B59**, 5770 (1999).

[39] I. S. Gradshteyn and I. M. Ryzhik, *Table of Integrals, Series, and Products, (Academic Press, 1965).*

[40] H. Haug, A. P. Jauho, *Quantum Kinetics in Transport and Optics of Semiconductors*, (Springer Verlag, Germany, 1996).

[41] Jagdeep Shah, *Ultrafast Spectroscopy of Semiconductors and Semiconductor Nanostructures*, (Springer-Verlag, Germany, 1996).